


Caspar, an adapter for VAPB and TER94, modulates the progression of ALS8 by regulating IMD/NF κ B-mediated glial inflammation in a *Drosophila* model of human disease

Shweta Tendulkar¹, Sushmitha Hegde^{1,†}, Lovleen Garg^{1,†}, Aparna Thulasidharan^{1,†}, Bhagyashree Kaduskar^{1,†}, Anuradha Ratnaparkhi² and Girish S. Ratnaparkhi^{1,*} 

¹Department of Biology, Indian Institute of Science Education and Research (IISER), Pune 411008, India

²Developmental Biology Group, MACS-Agharkar Research Institute, Pune 411004, India

*To whom correspondence should be addressed at: Indian Institute of Science Education and Research (IISER), Dr Homi Bhabha Road, Pashan, Pune 411008, India. Tel: +91 2025908053; Fax: +91 2020251566; Email: girish@iiserpune.ac.in

[†]Present address: Tata Institute for Genetics and Society (TIGS), Center at inStem, Bangalore, Karnataka 560065, India.

[‡]Equal contribution.

Abstract

Amyotrophic lateral sclerosis (ALS) is a fatal, late-onset, progressive motor neurodegenerative disorder. A key pathological feature of the disease is the presence of heavily ubiquitinated protein inclusions. Both the unfolded protein response and the ubiquitin-proteasome system appear significantly impaired in patients and animal models of ALS. We have studied cellular and molecular mechanisms involved in ALS using a vesicle-associated membrane protein-associated protein B (VAPB/ALS8) *Drosophila* model [Moustaqim-Barrette, A., Lin, Y.Q., Pradhan, S., Neely, G.G., Bellen, H.J. and Tsuda, H. (2014) The ALS 8 protein, VAP, is required for ER protein quality control. *Hum. Mol. Genet.*, 23, 1975–1989], which mimics many systemic aspects of the human disease. Here, we show that VAPB, located on the cytoplasmic face of the endoplasmic reticulum membrane, interacts with Caspar, an orthologue of human fas associated factor 1 (FAF1). Caspar, in turn, interacts with transitional endoplasmic reticulum ATPase (TER94), a fly orthologue of ALS14 (VCP/p97, valosin-containing protein). Caspar overexpression in the glia extends lifespan and also slows the progression of motor dysfunction in the ALS8 disease model, a phenomenon that we ascribe to its ability to restrain age-dependent inflammation, which is modulated by Relish/NF κ B signalling. Caspar binds to VAPB via an FFAT motif, and we find that Caspar's ability to negatively regulate NF κ B signalling is not dependent on the VAPB:Caspar interaction. We hypothesize that Caspar is a key molecule in the pathogenesis of ALS. The VAPB:Caspar:TER94 complex appears to be a candidate for regulating both protein homeostasis and NF κ B signalling, with our study highlighting a role for Caspar in glial inflammation. We project human FAF1 as an important protein target to alleviate the progression of motor neuron disease.

Introduction

Amyotrophic lateral sclerosis (ALS) is a human neurodegenerative disease that leads to the death of motor neurons. This disorder usually affects individuals late in life, with 90–95% cases being 'sporadic', indicating that the disease is not inherited. In about 5–10% of cases, the disease is 'familial', where the disease is inherited across generations (1–3). Despite the discovery of SOD1 as the first familial locus for ALS nearly three decades ago in 1993 (4,5), and the large volume of work, an understanding of the mechanistic aspects of disease initiation and progression has been elusive. One major reason for the delay has been the identification of more

than two dozen ALS causative loci in humans, with each locus being distinct and unrelated to each other in terms of their physiological function (6,7). For example, SOD1/ALS1 is primarily a regulator of cytoplasmic reactive oxygen species (ROS), Senataxin (SETX)/ALS4 (8) works as an RNA or DNA helicase, FUS/ALS6 (9) is a transcriptional activator, vesicle-associated membrane protein-associated protein B (VAPB/ALS8) (10) is an endoplasmic reticulum (ER) membrane resident single-pass protein that helps maintain intracellular membrane contact sites and KIFA/ALS25 (11) is a microtubule-based motor protein. Nonetheless, specific mutations in each of these genes lead to the development of the disease.

Received: January 10, 2022. Revised: March 25, 2022. Accepted: March 29, 2022

© The Author(s) 2022. Published by Oxford University Press. All rights reserved. For Permissions, please email: journals.permissions@oup.com

This is an Open Access article distributed under the terms of the Creative Commons Attribution-NonCommercial License (<http://creativecommons.org/licenses/by-nc/4.0/>), which permits non-commercial re-use, distribution, and reproduction in any medium, provided the original work is properly cited. For commercial re-use, please contact journals.permissions@oup.com

Whether the pathway leading to motor neuron death is distinct for each locus or is caused by convergence to a common downstream cellular mechanism is not completely clear. A universal mechanistic model for the disease should be able to explain the convergence to the common endpoint, by incorporating a related set of cellular pathways that are perturbed by each of the causative loci. This would presuppose that subsets of ALS causing genes are connected, being part of genetic sub-network(s) in the cell, regulating common or overlapping physiological functions. If true, then it should be possible to uncover genetic relationships between different ALS loci and link these interactions to a set of common cellular pathways. This is best done in animal models where genetic tools to elucidate such interactions exist. In the past decade, many such interactions have been discovered and cellular themes underscored. For example, multiple ALS loci have been found to be involved in functions related to RNA metabolism. These include *TDP-43*, *FUS*, *ATXN2*, *TAF15*, *EWSR1*, *hnRNPA1*, *hnRNPA2/B1*, *MATR3* and *TIA1*. Another common theme is proteostasis, involving both production of proteins—*TARDBP*, *FUS* and *TAF15* and degradation—*VCP*, *SQSTM1*, *UBQLN2*, *OPTN* and *CCNF*. Finally, vesicular transport, another potential fault line for ALS, involves *C9ORF72*, *VAPB*, *OPTN*, *CHMP2B*, *PFN1*, *TUBA4A*, *ANXA11*, *ATXN2*, *NEFH*, *PRPH*, *SPG11*, *SIGMAR1*, *GRN*, *DCTN1*, *KIF5A* and *ALSIN*. Further support for the genetic sub-network hypothesis is the finding that ALS is in all possibilities a polygenic disease with several genes contributing to initiation and progression in both sporadic (sALS) and familial (fALS) cases (12–14).

VAPB is a ubiquitous, tail anchored ER protein, enriched in contact sites where ER is juxtaposed with other intracellular membranes (reviewed in 15–17). VAPB associates with a number of partner proteins, reinforcing membrane–membrane distance and architecture (17) and also assisting in roles performed by its numerous interacting partners (15,17). Recent studies have focused on the elucidation of specific roles for VAPB with each individual protein (18–21), broadening our understanding of the workings of the VAPB network. VAPB was the 8th fALS locus to be discovered (10) and has been used to model the disease in both invertebrates (22–25) and vertebrates (26–28).

We have previously sought to uncover the gene regulatory network for the *Drosophila* orthologue of human VAPB, VAP33A/CG5014 (VAP here onwards) and to understand genetic relationships between ALS loci through an enhancer-suppressor screen (29). The study identified ALS orthologous loci (*SOD1*, *Alsin*, *TDP43*) as part of the VAP genetic network and also suggested an interaction with members of the Target of Rapamycin signalling pathway (29). We subsequently explored the genetic relationship between VAP and *SOD1* and found that *SOD1* regulation of cellular ROS levels led to a modulation of VAP^{P58S} aggregates (30), by triggering clearance of cellular inclusions via the

ubiquitin–proteasomal system (UPS). In the current study, we explore the relationship between VAP and transitional endoplasmic reticulum ATPase (*TER94/ALS14*; or *p97*, also called valosin-containing protein, *VCP*). The decision to explore this relationship in detail was on the basis of a targeted, tissue-specific genetic screen, described here, carried out in muscles, glia and motor neurons.

In our study, we find that Caspar, an orthologue of human Fas associated factor 1 (*FAF1*) (31,32), is a physical interactor of both VAP and *TER94* (33–35). We show that Caspar acts as a protein bridge, physically connecting VAP and *TER94*, which are orthologues of human *VAPB/ALS8* and *VCP/ALS14*, respectively. Interestingly, increased Caspar expression in glia can delay the onset of motor dysfunction, with Caspar negatively regulating Relish (*Rel*)/NF κ B signalling. Our findings suggest that glial Caspar plays a key role in disease progression by regulating age-dependent glial inflammation, thus highlighting the contribution of nonautonomous players in the development of the disease.

Results

A tissue-specific enhancer/suppressor screen suggests genetic interactions between VAP and *Drosophila* orthologues of ALS loci

In the past, we (29,30,36,37) and others (23–25,38–40) have used VAP^{P58S} overexpression (OE) models to understand the mechanisms of disease. Here, for our experiments, we chose an ALS8 disease model developed by Hiroshi Tsuda's laboratory (22), where an endogenous *genomic-VAP* (*gVAP* or *gVAP^{P58S}*) insert on the third chromosome is used to rescue the lethality of the VAP null (Δ VAP). The Tsuda disease model, Δ VAP;*gVAP^{P58S}*, unlike the control Δ VAP;*gVAP^{WT}*, has a shorter lifespan, shows progressive motor dysfunction, and has VAP^{P58S} inclusions in the brain with cells showing ER expansion and ER stress (22). In our laboratory, we have regenerated the Tsuda model, using the VAP Δ 166 allele instead of the VAP Δ 31 (see Materials and Methods) and have used this for our studies.

In order to study the genetic relationships between VAP and different ALS loci, we chose six *Drosophila* genes, each being an orthologue of a major fALS locus (Fig. 1A). The genes chosen are fly orthologues of human *TARDBP/ALS10*, *FUS/ALS6*, *SOD1/ALS1*, *VCP/ALS14* and *SETX/ALS4*, respectively. For each gene, transgenic lines for OE and knockdown (KD) experiments were procured (see Materials and Methods) and loss-of-function and gain-of-function experiments were conducted in the three tissues central to motor neuron disease, namely, neurons, muscle and glia. These experiments were driven by the concept that in addition to neuronal cells, non-neuronal cells (41) also contribute to the disease. Three drivers were chosen, one for each tissue, *myosin heavy-chain (MHC)-Gal4* for muscle, *reverse polarity (Repo)-Gal4* for glia and *OK6-Gal4* for motor neuron-specific expression.

FIGURE 1

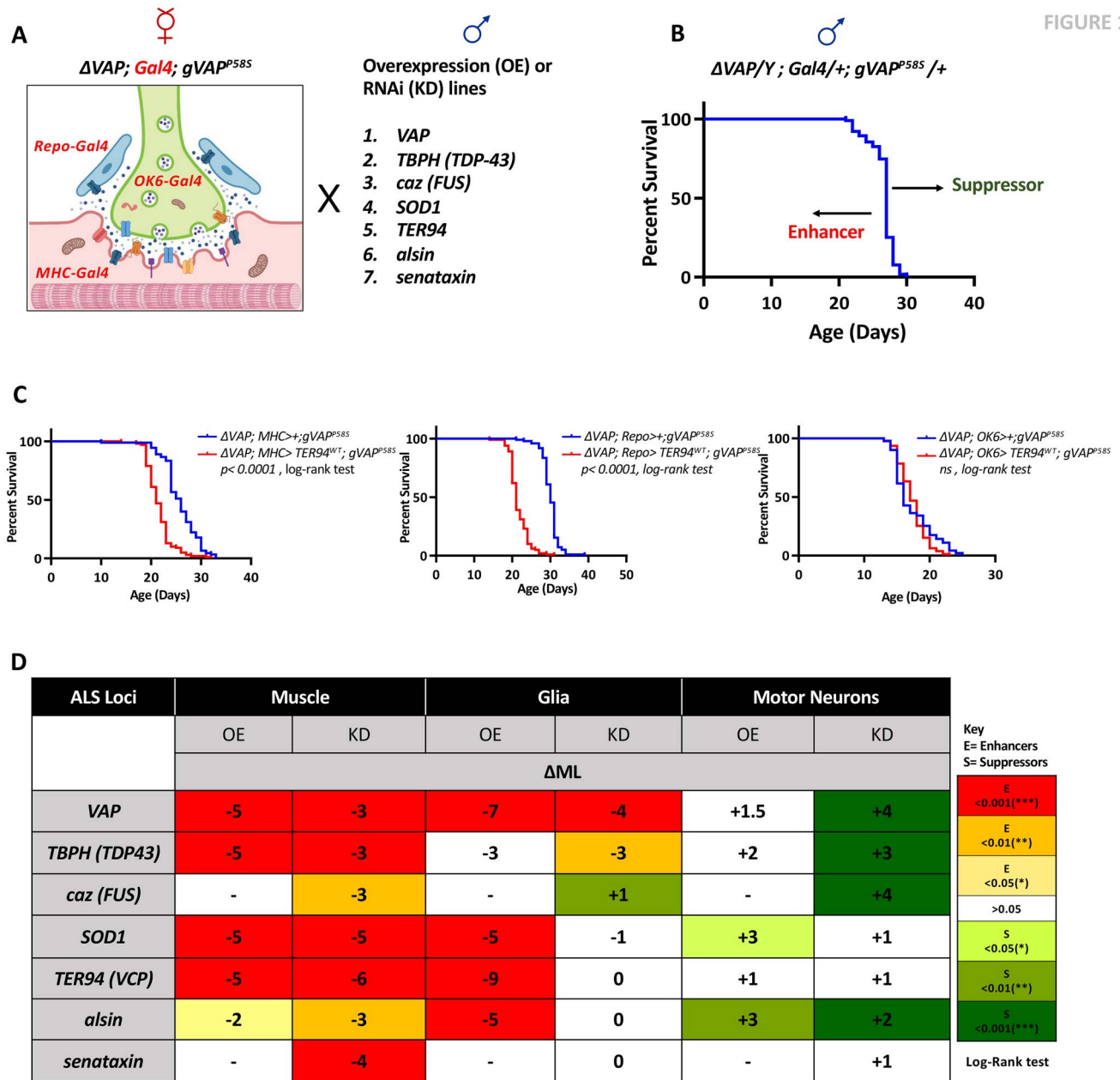


Figure 1. An enhancer/suppressor screen for genetic interaction between ALS orthologous loci in neurons, muscle and glia. (A) Tissue-specific expression in muscle ($\Delta VAP; MHC-Gal4; gVAP^{P585}$), glia ($\Delta VAP; Repo-Gal4; gVAP^{P585}$) and motor neurons ($\Delta VAP; OK6-Gal4; gVAP^{P585}$) was used to overexpress and KD VAP, TBPH, caz, SOD1, TER94, alsin and senataxin. (B) A schematic for monitoring the survival of male animals emerging from the crosses described in (A). The blue curve represents the control $\Delta VAP/Y; X-Gal4/+; gVAP^{P585}/+$ fly line; i.e. $\Delta VAP/Y; MHC-Gal4/+; gVAP^{P585}/+$ for the muscle-specific screen, $\Delta VAP/Y; Repo-Gal4/+; gVAP^{P585}/+$ for the glial-specific screen and $\Delta VAP/Y; OK6-Gal4/+; gVAP^{P585}/+$ for the motor neuron-specific screen. A shift from the lifespan of the control to the right was defined as a 'suppression' of the phenotype, whereas towards the left as 'enhancement'. The survival analysis was done using the log-rank test survival assay protocol, in Prism 7, over the entire dataset, where each curve was compared with the control and the value of significance was noted. This number is reported (Supplementary Material, Fig. S1) and is represented as a colour code in (D). Additionally, we considered values of ΔML [Change in ML] = ML (Experiment) - ML (Control) as a simple readout of enhancement or suppression. (C) Representative graphs for muscle, glial and motor neuronal OE of TER94. The red curve represents the locus studied (TER94). The P-value from the log-rank test listed in each graph is the comparison of the red curve with the blue curve (control). The muscle and glial OE of TER94 exhibits enhancement of lifespan defect ($P < 0.0001$; log-rank test), whereas motor neuronal expression shows no significant change. A complete set of graphs (muscle, glia, neurons) for KD and OE of all seven genes can be found in Supplementary Material, Figure S1. (D) Tabular summary of the tissue-specific screen highlights differential interaction of genetic loci with VAP^{P585}. The numbers in each cell indicate the ΔML , whereas the colours indicate different levels of statistical confidence, as per the log-rank test. The 'red-yellow tones' mark Enhancers (E), whereas the 'green tones' represent the same for Suppressors (S). '-' in the cell indicates that the experiment was not carried out. The caz OE construct is an insert on the X chromosome of the fly line and hence could not be used for male-specific assay, whereas for senataxin, the OE line was not available. 'OE' stands for overexpression using UAS lines and 'KD' stands for KD, using RNA interference.

Gal4 drivers for glia, muscle and neurons with insertions in the second chromosome were balanced with ΔVAP and $gVAP^{P585}$ to generate the following lines:

$\Delta VAP; Repo-Gal4; gVAP^{P585}$, $\Delta VAP; OK6-Gal4; gVAP^{P585}$, $\Delta VAP; MHC-Gal4; gVAP^{P585}$ (Fig. 1A). Gal4 carrying female flies were crossed to OE or KD(RNAi) lines of VAP, TBPH,

FUS, *SOD1*, *TER94*, *ALSIN* and *SETX*. Adult males in the F1 generation, which lacked functional VAP on the X chromosome (Δ VAP; Fig. 1B), were collected and subjected to lifespan analysis as described in Materials and Methods. Survival graphs for each cross are shown in Supplementary Material, Fig. S1 (representative graphs in Fig. 1C), with a summary tabulated in Figure 1D. Statistical analysis using the log-rank test, as detailed in Materials and Methods, was used to compare experimental lifespan curves with controls and change (Δ) in median lifespan (ML) was used as a simple parameter to reflect an increase (+) or decrease (–) in lifespan (Fig. 1D).

A summary of the results (Fig. 1D) of the differential lifespan analysis (data in Supplementary Material, Fig. S1), is as follows. In the muscle, both decrease and increase in activity of the genes tested seem to enhance the lifespan phenotype with a concomitant decrease in ML. In glia, increased activity of most of the genes (*VAP*, *SOD1*, *TER94* and *alsin*) tested seems to enhance the phenotype with a decrease in ML. In the KD studies, *VAP* and *TBPH* lead to a decrease in ML whereas for other genes, the changes in lifespan were not very significant. In neurons, the overall trend pointed to a suppression of the phenotype, with an increase in ML for KD of *VAP*, *TBPH*, *caz* and *alsin*. *SOD1* OE, as also *alsin* OE led to a mild suppression of the phenotype. For most other genes, the effect was not significant ($P > 0.05$). The small but significant increase in lifespan for *VAP* KD for motor neurons is unexpected, but may be a consequence of reduced levels of VAP, post RNAi, leading to decreased VAP aggregation overall. VAP aggregation being a concentration-dependent phenomenon, the enhanced survival suggests that reasonable amounts of active VAP are available in the cell.

The strongest enhancement of the lifespan phenotype was observed for *TER94* OE in glia with a Δ ML ranging from 7 to 10 days; *TER94* KD, in contrast, did not influence the lifespan of the Δ VAP/Y; *Repo-Gal4/+*; *gVAP^{P585}/+* line significantly (Fig. 1C and D). This result prompted us to explore, in greater detail, the *TER94*:VAP interaction, using our disease model. This direction was supported by a study from Gabriela Alexandru's group (35), which suggested that VAPB and VCP could interact physically in mammals via FAF1. As a first step, we conducted affinity purification experiments using fly lysates to test if VAP was a physical interactor of Caspar and if so, whether Caspar could be a potential adapter for the VAP:TER94 interaction in our disease model.

Caspar is a physical interactor of both VAP and TER94

A sequence comparison of Caspar with FAF1 finds that both proteins are of similar size, have the same domain structure (Fig. 2A) and on sequence alignment show 54% sequence similarity overall with ~34% identity. Like its mammalian orthologue, Caspar contains well-characterized, N-terminal, ubiquitin-associated

(UBA; SM00165) domain, known to interact with poly-ubiquitinated proteins and a C-terminal 'Ubiquitin regulatory X' UBX domain (SM00166), a known VCP/TER94 interactor (48). As detailed earlier (35), the Caspar superfamily is conserved from flies to humans and incorporates a variant of FFAT, 'two phenylalanines in an acidic tract' motif, EFFDAXE, (42,43). It is well established that this motif mediates interaction with VAP (15,37,42). Consistent with this, deletion or modification of this motif led to disruption of the FAF1:VAPB interaction (35). This strongly suggests that *Drosophila* Caspar, which contains a similar highly conserved FFAT motif (Fig. 2A, lower panel, Underlined), may also be a VAP interactor.

To test the VAP:Caspar interaction, we used an anti-Caspar antibody developed in our laboratory, as described in Materials and Methods, to immunoprecipitate (IP) Caspar and its interactors. The anti-Caspar antibody specifically recognizes an ~85 kDa band in adult whole animal lysates (Supplementary Material, Fig. S2A), which is not seen in lysates of homozygous *caspar^{lof}* animals (Supplementary Material, Fig. S2A). The anti-Caspar antibody IPs could enrich Caspar, as visualized by western blotting (Fig. 2B; *, top panel) and could also pull down VAP (Fig. 2B; **, bottom panel). To identify other Caspar interactors, we processed the Caspar IPs from adult and embryonic lysates through a Mass Spectrometer and found that Caspar associates with cytoplasmic proteins involved in protein folding/unfolding and ubiquitin (Ub)-mediated degradation (Fig. 2C; Supplementary Material, Fig. S2E). In embryonic lysates, which is a rich source of Caspar, VAP is found as the second most enriched protein (after TER94), on the basis of peptide count. In fly head extracts, the anti-Caspar antibody enriches both Caspar (Fig. 2D; *, top panel) and VAP (Fig. 2D; **, bottom panel). Further support for the VAP:Caspar interaction came from a 'reverse IP' experiment in fly heads, where a VAP IP could pull down Caspar (Supplementary Material, Fig. S2C). In S2 cell extracts, anti-Caspar pull downs, in addition to enriching Caspar, also enrich VAP and TER94 (Supplementary Material, Fig. S2D) suggesting that these interactions are conserved across different cell types. The VAP:Caspar physical interaction and the list of associated proteins such as TER94, Ufd1-like and Npl4 give credence to the idea that Caspar acts as an adapter to bring together VAP and TER94 for an important physiological function, possibly related to protein homeostasis and degradation. Caspar is thus a bona fide interactor of both VAP and TER94, and this protein complex is conserved from flies (VAP:Caspar:TER94) to humans (VAPB:FAF1:VCP; BARON *et al.*, 2014).

Expression of Caspar in the glia extends lifespan

The existence of a VAP:Caspar:TER94 complex in flies suggests that TER94 and Caspar may have common or overlapping physiological roles. In order to uncover these, we expressed two ALS fly variants of *TER94*, *TER94^{A229E}* and *TER94^{R152H}* (44,45) in the glia, muscle and neurons.

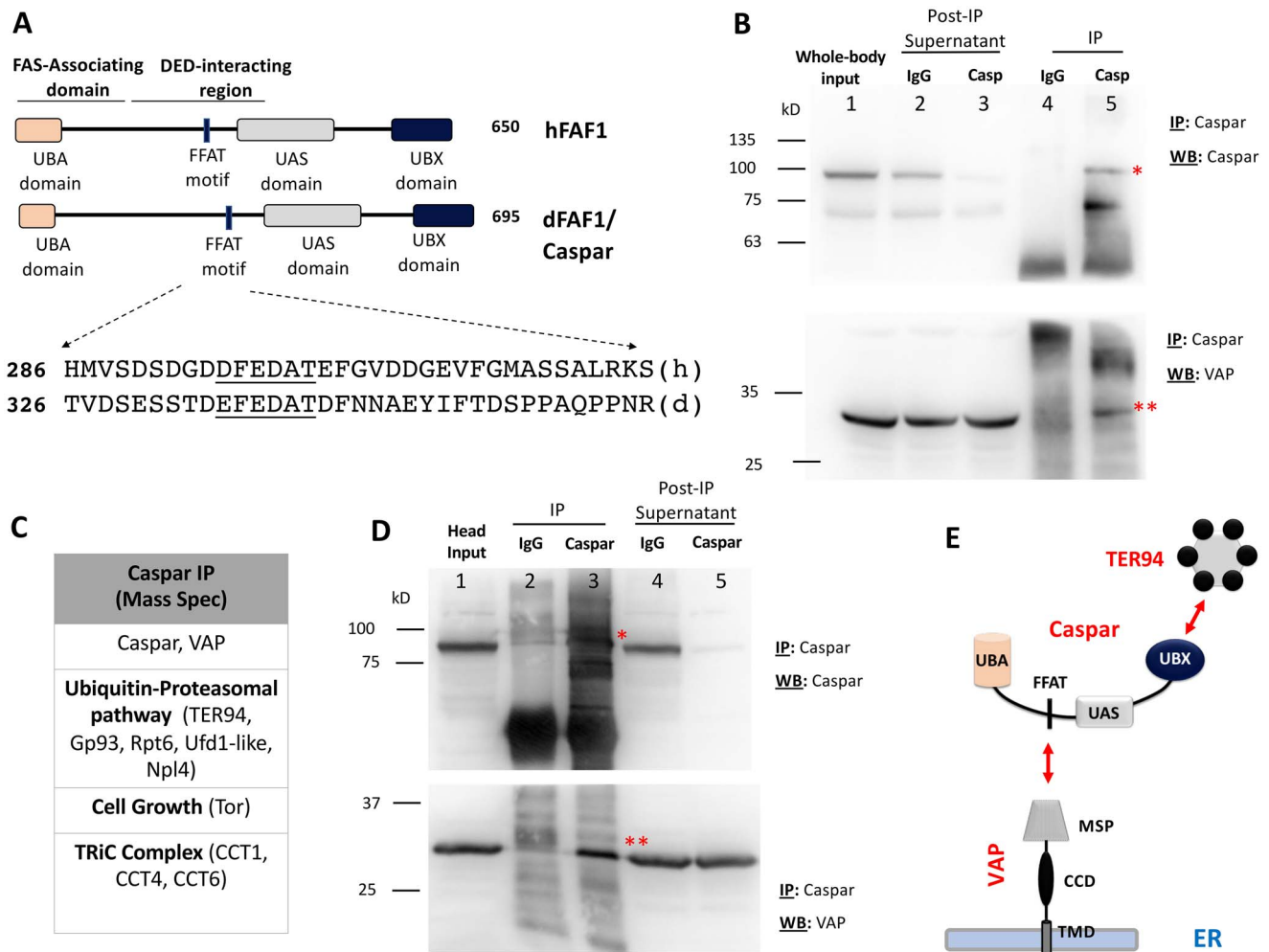


Figure 2. *Drosophila* Caspar is a physical interactor of VAP and TER94. (A) *Drosophila* Caspar is an orthologue of human FAF1. The conserved N-terminal Ub-interacting and C-terminal TER94 interacting domains suggest roles for Caspar as an adapter in the proteasomal degradation. A conserved FFAT motif (amino acids underlined), which is a well-characterized VAP interactor is present in both polypeptides. This suggests that FFAT motif in Caspar may be the interface for an interaction with VAP. (B) An antibody against full-length Caspar was generated (see Materials and Methods) and validated (Supplementary Material, Fig. S2). When used for IP of whole animal lysates, the Rb Caspar antibody could affinity-purify Caspar (*, 90 kDa, lane 5, top panel) and also VAP (**, 25 kDa, lane 5, bottom panel). A concomitant decrease in Caspar in the supernatant (lane 3, top panel) is also seen, post IP. The ~70 kDa reactive band is a feature of Caspar westerns and is in all probability is a nonspecific band. (C) TER94, Gp93, Rpt6, Tor, CCT1 and CCT4 are detected by mass spectrometry in the Caspar antibody immune-precipitates, using whole-body and embryonic lysates (Supplementary Material, Fig. S2E). Many of these proteins are functionally associated with the UPS. (D) Caspar immune precipitates using fly head lysates confirm that Caspar (*) is expressed in the head and can be enriched by the Caspar antibody (lane 3, top panel). Also, VAP (**) is a Caspar interactor (lane3, bottom panel). A concomitant decrease in Caspar in the supernatant (lane 5, top panel) is seen, post IP. Further support for the Caspar:VAP interaction comes from a 'reverse' IP experiment where an anti-VAP antibody is used for IP and Caspar is enriched (Supplementary Material, Fig. S2C). (E) A model for the interaction of VAP, an ER resident membrane protein, with cytoplasmic Caspar. Mass spectrometry and other (Supplementary Material, Fig. S2D and E) interaction data suggest that TER94 and other proteins of the UPS are part of a Caspar protein:protein interaction network in the cell.

Expression of *TER94*^{R152H} led to a significant extension of lifespan ($\Delta\text{ML} = +4.5$) when expressed in glia, but not in muscle ($\Delta\text{ML} = -2$) or neurons ($\Delta\text{ML} = +2$). *TER94*^{A229E} expression in the glia was lethal and adult flies did not emerge (Fig. 3A). R152 is located in the N-terminal CDC48 domain of TER94 and R152H is classified as a dominant active allele (44,46). The N-terminal domain of TER94 is also known to interact with UBX domains, suggesting that the mutation may modulate the strength or dynamics (46) of the TER94:Caspar interaction. In order to test the effect of OE and KD of Caspar in glia, we procured an RNAi line for *caspar* (*UAS-caspar*^{RNAi}) and also generated *UAS-caspar* lines (see Materials and Methods). $\Delta\text{VAP}; \text{Repo-Gal4/+}; g\text{VAP}^{\text{P58S}}/\text{UAS-caspar}^{\text{RNAi}}$ males had

a shorter lifespan ($\Delta\text{ML} = -4.0$) when compared with the disease model, $\Delta\text{VAP}/Y; \text{Repo-Gal4/+}; g\text{VAP}^{\text{P58S}}/+$ (Fig 3A and B). Intriguingly, OE of *caspar* in the glia ($\Delta\text{VAP}; \text{Repo-Gal4/+}; g\text{VAP}^{\text{P58S}}/\text{UAS-caspar}$) significantly increased lifespan ($\Delta\text{ML} = +7.5$) (Fig. 3B) of the disease model. In repeat experiments, ΔML ranged from 7 to 9 days, with the extension of lifespan always greater than $\Delta\text{VAP}; \text{Repo-Gal4/+}; g\text{VAP}^{\text{P58S}}/\text{UAS-TER}^{\text{R152H}}$ where the ΔML ranged from 4 to 6 days. The dramatic increase was made even more significant because OE of *caspar* in a wild-type background (Fig. 3C and D) severely shortened lifespan ($\Delta\text{ML} = -17$) (Fig. 3D), whereas *caspar* KD increased lifespan ($\Delta\text{ML} = +4$). For TER94, both OE and KD decreased ML, in wild-type animals, by 3.5 and 9 days, respectively,

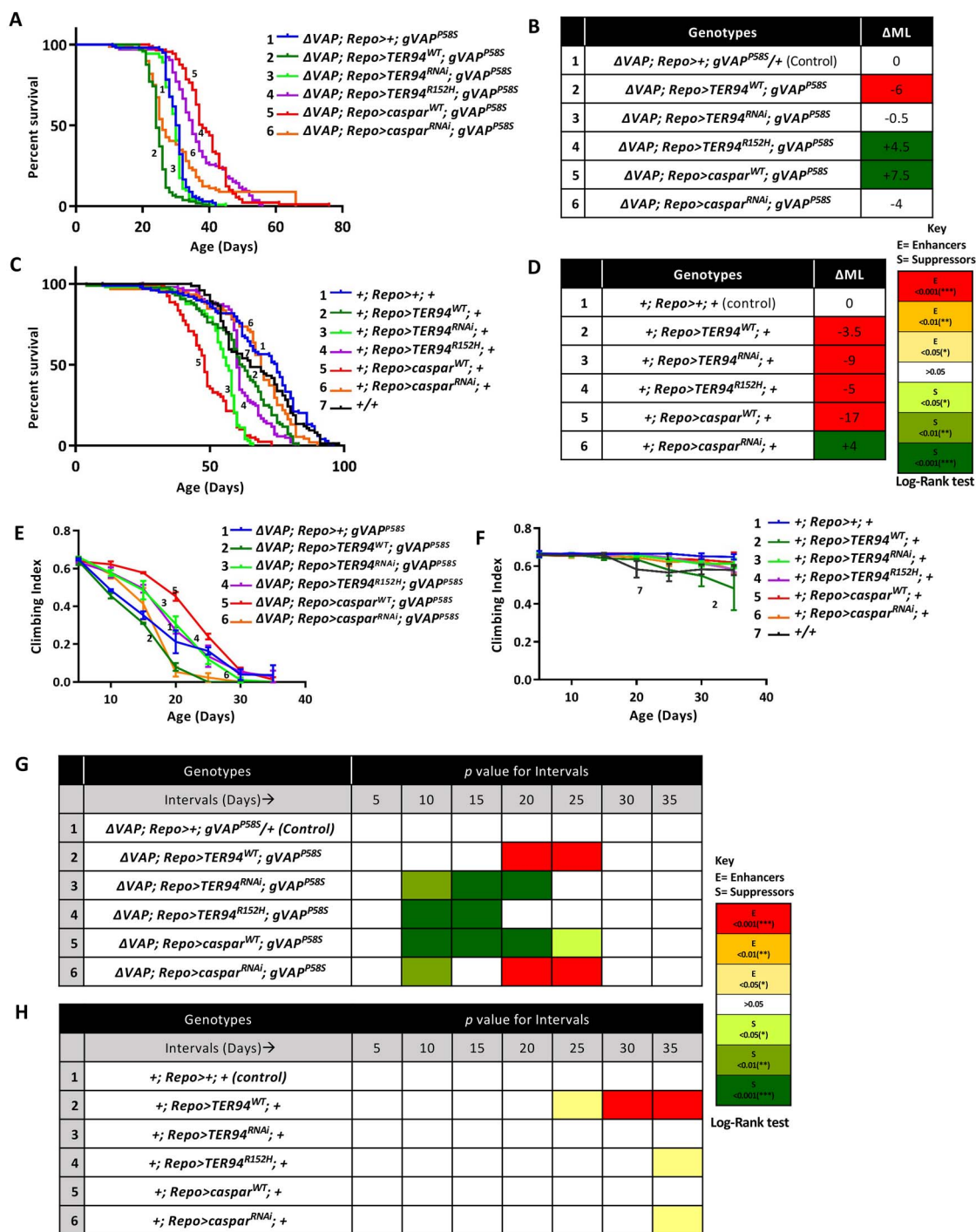


Figure 3. OE of *caspar* in the glia increases lifespan and delays motor dysfunction in the disease model. **(A)** Lifespan curves for OE of *TER94*^{WT} (2, dark green curve), *TER94*^{RNAi} (3, light green), *TER94*^{R152H} (4, purple), *caspar*^{WT} (5, red) and *Caspar*^{RNAi} (6, orange). Δ VAP/Y; Repo>+; gVAP^{P58S}/+ (1, blue, ML = 30.5 days) was used as the control. $n \sim 100$ flies for every genotype. Curve comparison was done using the log-rank test. Combined P-value for the whole set is <0.001. For both *TER94*^{R152H} and *caspar*^{WT} OE, there is an increase in lifespan. **(B)** Tabulated results for lifespan recordings in (A), quantified in the form of Δ ML. The colour codes are as described previously (Fig. 1D). **(C)** Lifespan curves for OE of *TER94*^{WT} (2, dark green curve), *TER94*^{RNAi} (3, light green), *TER94*^{R152H} (4, purple), *caspar*^{WT} (5, red) and *caspar*^{RNAi} (6, orange) using +; Repo>Gal4; + background. +; Repo>+; + (Curve 1 in blue colour, ML = 75) was the control for curves 2–6, whereas +/+ (wild-type flies, black curve, 7) was used as the master control (ML = 65 days) to compare with curve 1 ($P > 0.05$, not significant). **(D)** Functions as the control for the respective gene-specific expressions in (A). $n \sim 100$ flies for every genotype. Curve comparison was done using the log-rank test. Combined P-value for the whole set is <0.001. **(E)** Tabulated results for lifespan recordings in (C), quantified in the form of Δ ML. The colour codes are as described previously. **(F)** Climbing indices for glial OE of *TER94*^{WT} (2, dark green curve), *TER94*^{RNAi} (3, light green), *TER94*^{R152H} (4, purple), *caspar*^{WT} (5, red) and *caspar*^{RNAi} (6, orange). Δ VAP; Repo>+; gVAP^{P58S}/+ (1, blue colour) was used as the control. The individual P-values are listed in (G). For both *TER94*^{R152H} and *caspar*^{WT} OE, there is an age-dependent improvement in motor function. **(H)** Climbing indices for glial OE of *TER94*^{WT} (2, dark green curve), *TER94*^{RNAi} (3, light green), *TER94*^{R152H} (4, purple), *caspar*^{WT} (5, red) and *caspar*^{RNAi} (6, orange) in the wild-type background. +; Repo>+; + (1, blue colour) was the control for curves 2–6. The individual P-values are listed in (H). +/+ (wild-type flies, black curve, number 7) was used as the master control to compare curve 1, the P-values for this comparison were as follows: Day 5, $P > 0.05$ (ns, not significant),

pointing to the importance of maintaining homeostatic levels of TER94 in the glia. Thus, the increased lifespan seen after *TER94^{R152H}* and *caspar^{WT}* glial OE suggests important physiological roles for Caspar and TER94 in our disease model.

Expression of Caspar in the glia delays age-dependent motor deterioration

The Δ VAP; *gVAP^{P58S}* fly line develops progressive motor defects (22) (Fig. 3E). As OE of both the *TER94^{R152H}* and *caspar* increases the lifespan of the *VAP^{P58S}* disease model, we measured the changes seen in motor activity, using the ability of flies to climb as a readout. The data were measured and analyzed as described (see Materials and Methods) and displayed in terms of a climbing index (Fig. 3E and F). *Caspar* OE significantly improved motor function (Fig. 3E, 5—red line), when compared with the control (Fig. 3E, 1—dark blue curve). *TER94^{R152H}* OE also showed a mild improvement in motor function, at par with *TER94 KD*. In comparison, when expressed in a wild-type fly, motor function did not improve for any of the genotypes (Fig. 3F) tested, with the possible exception of *TER94 OE* (Fig. 3F, 2—dark green curve). To better appreciate the age dependence on motor function, we have plotted the data at 5-day intervals (Fig. 3G and H; Supplementary Material, Fig. S3A and B). In Figure 3G and H, the statistical significance is colour coded, with yellow, orange and red signifying deterioration of motor function, and shades of green indicating improvement in motor function, for animals of equivalent age. For the disease model (Fig. 3G), in the age group 10–20 days, there appears to be a significant improvement of motor function for *TER94^{R152H}*, *TER94 KD* and *caspar OE*. In contrast, OE of *TER94^{WT}* and *caspar RNAi* led to a significant deterioration of motor function for flies aged 20 and 25 days. For wild-type flies, *TER94^{WT}* OE was detrimental to motor function after 25 days (Fig. 3H).

Both the lifespan and motor dysfunction data suggest that the VAP:Caspar:TER94 complex or its constituents may be an important contributor to the progression of the disease in glia. TER94 is an important member of the UPS that leads to proteasomal degradation of proteins (47,48). With Caspar having an ability to coordinate the transfer of ubiquitinated proteins to TER94, and with VAP acting as a docking site for Caspar, there is a strong possibility that these proteins cooperate in a physiological function that is related to proteostasis. This common function may be the endoplasmic-reticulum associated degradation (ERAD) (49–51) or clearance of *VAP^{P58S}* inclusions/aggregates (30). To confirm the same, we measured the change in the inclusion status of VAP aggregates in the brain of the

adult fly, in response to *caspar OE*, in an age-dependent manner.

Caspar expression does not modulate VAP^{P58S} inclusions in the adult brain

In an earlier study, working with the larval brain, we had uncovered the physiological basis of the genetic interaction between SOD1/ALS1 and VAP/ALS8 (29,30). Cellular ROS, when increased in response to SOD1 malfunction, triggered proteasomal activity, which led to a clearance of *VAP^{P58S}* aggregates from brain cells. The density of *VAP^{P58S}* inclusions in the brain was measured and found to decrease significantly with an increase in cellular ROS (30). A similar methodology was developed to measure aggregates in the adult fly brain of the disease model. Interestingly, the density or area of VAP inclusions in the brain did not increase or decrease significantly on *caspar OE* or even *caspar KD* in the glia (Fig. 4), in both larval (Supplementary Material, Fig. S4) and adult brains (Fig. 4). This would suggest that the increased lifespan and improved motor function that we see are not related to the 'average' density or size of *VAP^{P58S}* inclusions, which can be visualized by microscopy. This suggests that Caspar may either modulate proteostasis of proteins other than VAP inclusions or it may suggest that it has other, unknown functions in the cell.

In the literature, the only known function in fly literature for Caspar relates to its role in inflammation (52). Caspar negatively regulates immune deficient (IMD)/NF κ B signalling by controlling the activity of the protease Death-related ced-3/Nedd2-like caspase (Dredd), a Caspase-8 orthologue (53,54), which in turn cleaves the full-length precursor Relish (Rel), a fly NF κ B, which is sequestered in the cytoplasm. FAF1 (55), the mammalian orthologue of Caspar has similar roles in NF κ B signalling (56,57), negatively regulating signalling by influencing the I κ B kinase (IKK) complex. OE of FAF1 in Jurkat cells causes cell death, a phenomenon that is dependent on its interaction with Fas-associated death domain (FADD) and Caspase-8 (32). Dredd was itself discovered as a novel effector for apoptosis (58) and is a FADD interactor (59). Cleavage of Rel generates an N-terminal 68 kDa polypeptide (REL68) that can be transported to the nucleus and transcriptionally activate defence genes. An increase in Caspar activity leads to a reduction in IMD signalling whereas the absence of Caspar leads to hyper-activation of IMD signalling and hence inflammation (52) in immune cells.

Given the role of Caspar in regulating inflammation, we hypothesize that an increase in inflammation in our ALS8 disease model may be contribute to its short lifespan and poor motor abilities. OE of Caspar would relieve inflammation, consequently improving lifespan

Day 10, $P > 0.05$ (ns), Day 15, $P > 0.05$ (ns), Day 20, $P > 0.01$ (**), Day 25, $P > 0.001$ (***) , Day 30, $P > 0.05$ (*) and Day 35, $P > 0.05$ (*). (G) Individual P -values for intervals (5 days) for the climbing index of the animals in the Δ VAP; *Repo-Gal4*; *gVAP^{P58S}* background are plotted as a colour code. As compared with control (row 1), *caspar^{WT}* OE leads to improved motor activity in the age range 10–25 days, whereas for *TER94^{R152H}*, the period is 10–15 days. (H) Individual P -values for intervals (5 days) for the climbing index of the animals in the *Repo-Gal4* background. As compared with control (row 1), *caspar^{WT}* OE does not improve motor activity in the age range 1–30 days.

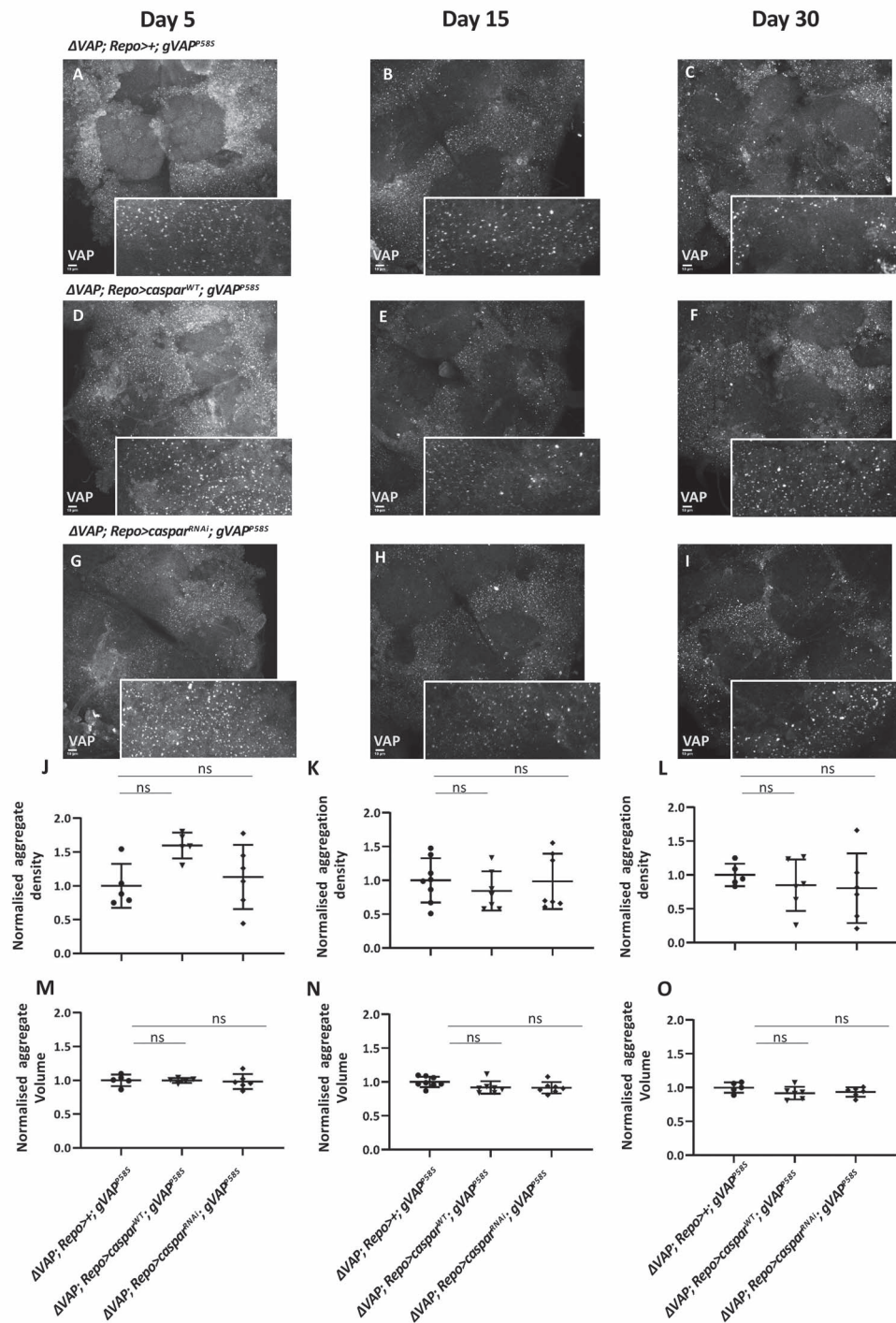


Figure 4. VAP inclusions in the brain of adult animals maintain *status quo* in response to *caspar* OE. Representative images of VAP protein inclusions in adult brains for days 5, 15 and 30. The inclusions are marked with an anti-VAP antibody. The scale bar for the image is 10 μm . The inclusions are highlighted (2 \times digital zoom) in the inserted panel for each image. (A–C) $\Delta\text{VAP}; \text{Repo}>+; g\text{VAP}^{\text{P58S}}$, (D–F) $\Delta\text{VAP}; \text{Repo}>\text{caspar}^{\text{RNAi}}; g\text{VAP}^{\text{P58S}}$, (G–I) $\Delta\text{VAP}; \text{Repo}>\text{caspar}^{\text{WT}}; g\text{VAP}^{\text{P58S}}$. (J–O) Graphical representation of normalized ‘aggregate density’ (J–L) and normalized ‘aggregate volume’ (M–O) of VAP inclusions, as defined in Materials and Methods. The genotypes compared are $\Delta\text{VAP}; \text{Repo}>+; g\text{VAP}^{\text{P58S}}$ and $\Delta\text{VAP}; \text{Repo}>\text{caspar}^{\text{RNAi}}; g\text{VAP}^{\text{P58S}}$. $n = 5\text{--}10$ brain samples. One-way ANOVA followed by Tukey’s multiple comparison (* $P < 0.05$, *** $P < 0.001$, **** $P < 0.0001$; ns, not significant). Error bars indicate s.d.

and motor function. If so, we predict that there should be increased inflammation in the disease model, especially in older flies and that modulation of the IMD/Rel signalling in glia should suppress or enhance the lifespan and improve age-dependent motor function.

Progression of ALS8 is modulated by the extent of glial inflammation

Healthy ageing in *Drosophila* includes the age-dependent upregulation of the immune response (60), regulated by the IMD/Rel pathway and is strongly observed in the

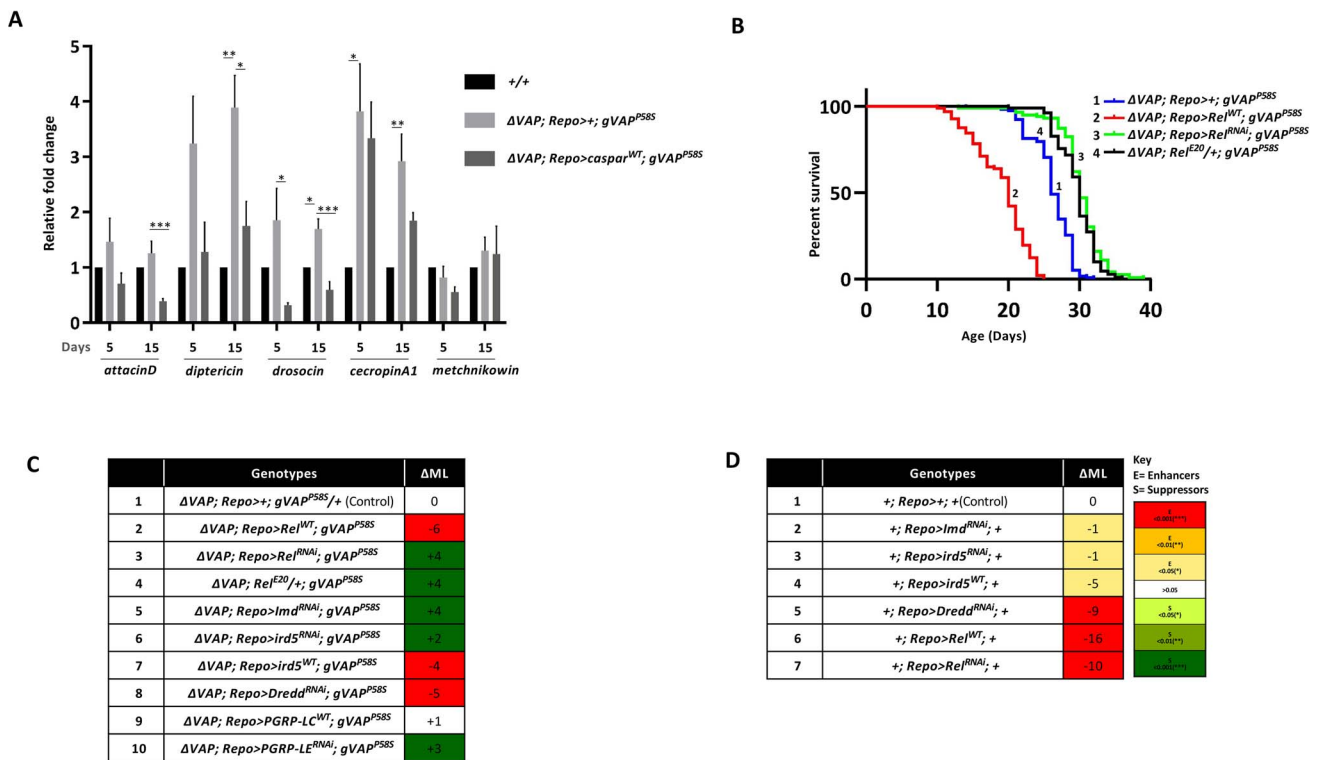


Figure 5. Inflammation in glia, regulated by IMD/Rel signalling contributes to the progression of the disease. **(A)** Expression of Rel target genes *attacinD*, *dipteracin*, *drosocin*, *cecropinA1* and Toll pathway target *metchnikowin* in day 5 and day 15 adult heads of wild-type (+/+), ΔVAP ; *Repo*>+; *gVAP*^{P58S} and ΔVAP ; *Repo*>*caspar*^{WT}; *gVAP*^{P58S} lines. Values on the Y-axis depict the fold-change normalized to the housekeeping gene *rp49*. Values shown are mean \pm SEM. *N* = 3, *n* = 3. Statistical analysis by two-way ANOVA followed by Tukey's multiple comparison test. **P* < 0.05, ***P* < 0.01, ****P* < 0.001. **(B)** Lifespan plots for OE of *REL*^{WT} (2, red curve), *Rel*^{RNAi} (3, light green), *REL*^{E20} (4, black) in the ΔVAP ; *Repo*-Gal4; *gVAP*^{P58S} genetic background. ΔVAP ; *Repo*>+; *gVAP*^{P58S}/+ (1, blue curve) was used as the control. Curve comparison was done using the log-rank test. Combined *P*-value for the whole set is <0.001. **(C)** Tabulated results (Δ ML) for lifespan recordings for experiments displayed in (B) and [Supplementary Material, Fig. S5A](#). Levels of statistical confidence are colour coded. ML for control, ΔVAP ; *Repo*>+; *gVAP*^{P58S}/+, is 26 days. **(D)** Tabulated results (Δ ML) for lifespan recordings for controls as shown in [Supplementary Material, Figure S5B](#). Levels of statistical confidence are colour coded.

fly head (60). We measured inflammation in the brain by measuring the levels of mRNA for Imd/Rel targets such as *attacinD*, *dipteracin*, *drosocin* and *cecropinA1* and a Toll/Dif target *metchnikowin*, in the dissected heads of adult *Drosophila*, as a function of age. At day 5, ΔVAP ; *Repo*>+; *gVAP*^{P58S} heads had *dipteracin* and *attacinD* levels with higher averages, but not statistically significant. For 5-day-old animals, *drosocin* and *cecropinA1* levels were significantly higher than age-matched control flies (Fig. 5A). For 15-day-old animals, where the disease had progressed, compared with age-matched animals, there is a 2–4-fold increase in mRNA levels for *dipteracin*, *drosocin* and *cecropinA1*. For *attacinD*, *dipteracin* and *drosocin*, OE of *caspar* in the glia reduces levels of these antimicrobial peptide genes, by ~2-fold. *Metchnikowin*, a target of Toll signalling does not show age-dependent inflammation and is not influenced by *caspar* OE (Fig. 5A). Thus, on the 15th day, with disease onset well underway, and with ~80% of the animals still alive, we observed a significant increase in inflammation in the head, which is reined in by Caspar.

To test the second prediction, we modulated the levels of IMD/Rel signalling to upregulate or downregulate glial inflammation. Enhanced inflammation should lead to a reduction in ML and reduction in inflammation

should increase the ML of the disease model. First, we measured the change in lifespan of ΔVAP ; *Repo*>+; *gVAP*^{P58S} flies after overexpressing and knocking down *Rel*, the transcriptional effector of the IMD/Rel pathway. *Rel* OE leads to increased inflammation and reduced lifespan by ~6 days (Fig. 5B and C). KD of *Rel* by RNAi or reduction of *Rel* by ~50% (*Rel*^{E20}/+) increased Δ ML by ~4 days (Fig. 5B and C). Next, we tested other elements of the IMD/Rel pathway; KD of IMD, IRD5 and PGRP-LC showed an enhancement in lifespan by 2–3 days (Fig. 5C), suggesting that these genes were part of a sterile inflammation cascade and/or a feedback loop. OE of IRD5 decreased lifespan (Δ ML = -4), whereas OE of PGRP-LC did not modulate lifespan, whereas KD of PGRP-LE increased Δ ML by 3 days.

KD of *Dredd* reduced lifespan (Δ ML = -5). The *Dredd* result was unexpected as a reduction in *Dredd* activity should reduce *Rel* signalling and reduce inflammation. Control lifespan experiments ([Supplementary Material, Fig. S5](#); Fig. 5D), in wild-type flies demonstrate that both gain-of-function and loss-of-function of *Rel* activity shorten lifespan as does reduction of *Dredd* in the glia. *Dredd* loss of function may have a role in triggering cell death and thereby influencing inflammation. The single available *Dredd* RNAi stock (BDSC, 34070) appears to be

a weak and sick stock, and this may also confound the data. *Dredd* resides on the X chromosome, which makes it challenging to use *Dredd* deficiencies for our male-specific readout. Another possibility is that Rel cleavage in glia may be *Dredd* independent, with an alternative pathway used for Rel cleavage and import. For example, in mammals, NF κ B cleavage and maturation is a function of the proteasome (61), rather than a *Dredd* orthologue. Caspar, like FAF1 in mammals, may directly bind to and influence Rel maturation.

Caspar-mediated glial inflammation is independent of its physical interaction with VAP

Our data suggest that Caspar in the glia does not influence the clearance of aggregates in the brain, rather Caspar functions to regulate age-dependent inflammation via Rel signalling. Hence, an important question would be to determine if the ability of Caspar to regulate inflammation is dependent (or independent) on its interaction with VAP. In order to test this hypothesis, we generated mutants of Caspar where the FFAT-like motif (Fig. 2B) was mutated. Three independent mutants were generated; in the first experiment, the Phenylalanine in the FFAT-like motif was replaced by alanine (Caspar^{EFE} to Caspar^{EAE}), in the second all three residues were replaced by Alanine (Caspar^{AAA}), and in the third case, the stretch of seven 'EFEDATD' residues was deleted (Caspar^{ΔFFAT}). All three mutants were cloned and then expressed in stable S2R+ cell lines that were already expressing VAP:GFP (Lanes 1–5, Fig. 6A) and also had native Caspar expression (Fig. 6A, lane 1; Fig. 6C, lanes 1–2). An affinity pull-down experiment, using the rabbit anti-Caspar antibody, was performed on extracts of cells expressing all four constructs (Caspar^{WT}, Caspar^{EAE}, Caspar^{AAA} and Caspar^{ΔFFAT}), as individual cultures. We found that the antibody could efficiently IP Caspar (Fig. 6A, lanes 10–13 and 15, upper panel) in each case. However, the ability of each variant to interact with VAP:GFP was different. Caspar^{WT} could pull down VAP:GFP (lane 11, lower panel) effectively, but the pull-down for the different variants (lanes 12, 13, 15) was not as efficient, being at par with the mock pull-down in the no-transfection controls, suggesting that the Caspar:VAP interaction was weaker or disrupted in the mutants. It is to be noted that because Caspar dimerizes, the mutant Caspar could interact with the wild-type Caspar in S2 cells to form wild-type:mutant heterodimers. Thus, the small fraction of VAP:GFP seen in pull-downs conducted with mutant Caspar could be simply because of the interaction between native Caspar and VAP:GFP.

The next question was if the Caspar variants with a disrupted FFAT-like motif could suppress age-dependent inflammation. To test this, we generated UAS constructs (see Materials and Methods), for Caspar wild-type and two of the three FFAT-like variants. Transgenic flies for UAS-Caspar^{WT}, UAS-Caspar^{AAA} and UAS-Caspar^{ΔFFAT} were generated, with inserts on the third chromosome (Attp2 docking site), followed by validation of expression

of these lines. The lines were expressed in glia, as in previous experiments, and levels of *dipt* monitored, 5 and 15 days post-eclosion. We find that Caspar^{AAA} was able to suppress post-inflammation on par with Caspar^{WT} (Fig. 6B). Casp^{ΔFFAT} could only do so at 50% of wild-type levels, and this may simply be because the deletion of seven amino acids may significantly destabilize the folded state of Caspar and reduce its function. Overall, our data suggest that interaction with VAP is not essential for Caspar's ability to regulate Rel-mediated inflammation.

We also tested the interaction of VAP and VAP^{P58S} with Caspar, in S2R+ cells. We expressed Caspar in stable cell lines expressing VAP:GFP and VAP^{P58S}:GFP and performed an immunoprecipitation (IP) experiment using the anti-Caspar antibody (Fig. 6C). As a significant fraction of VAP^{P58S} would be in cytoplasmic inclusions, not amenable to solubilization in our cellular extracts, drawing conclusions from this experiment is not straightforward. Nevertheless, we see that Caspar does pull down VAP^{P58S}, albeit at levels lower than that of VAP. On the basis of this evidence, Caspar does not appear to lose its ability to interact with VAP in the VAP^{P58S} variant.

In summary, IMD/Rel signalling (reviewed in 62–65), in the glia, appears to play a major role in regulating the age-dependent deterioration and motor function of our disease model. Caspar can negatively regulate IMD/Rel signalling in glial cells and alleviate the disease by reducing inflammation in the brain. Caspar's interaction with VAP appears not to be essential for its ability to restrain inflammation.

Discussion

Over the past decade, it has become apparent that NF κ B signal transduction cascades have diverse roles in the brain (reviewed in 66–68). Major functions of NF κ B signalling include the regulation of the neuronal immune response (69,70), learning and memory (71), neural development (72–75) and neuronal cell death (76). In flies, the Toll/NF κ B pathway has been linked to regulation of post-synaptic Glutamate receptor (GluRIIA) levels (77), whereas the IMD/NF κ B signalling appears to have important behavioural, apoptotic (76) and neuro-inflammatory roles (60,78–80). In 2017, the Ligoxygakis laboratory (60) found that IMD/NF κ B signalling in the *Drosophila* brain was important for a normal lifespan, with negative regulators of IMD/NF κ B playing critical roles in reducing inflammation in the brain. Enhanced inflammation was a key feature in age-dependent neurological decline. Reduction of inflammation, specifically in the glia, could reverse phenotypes associated with age-dependent neurodegeneration. In agreement with this idea, lifespan in a fly model of Spinocerebellar ataxia (SCA, 80), where SCA3^{polyQ78} was expressed in neurons, could be extended by reduction of IMD/Rel signalling. Earlier, in a SOD1^{G93A} mouse model for ALS (81), it was found that NF κ B signalling is upregulated in spinal cords, a feature also seen in the same tissue in human

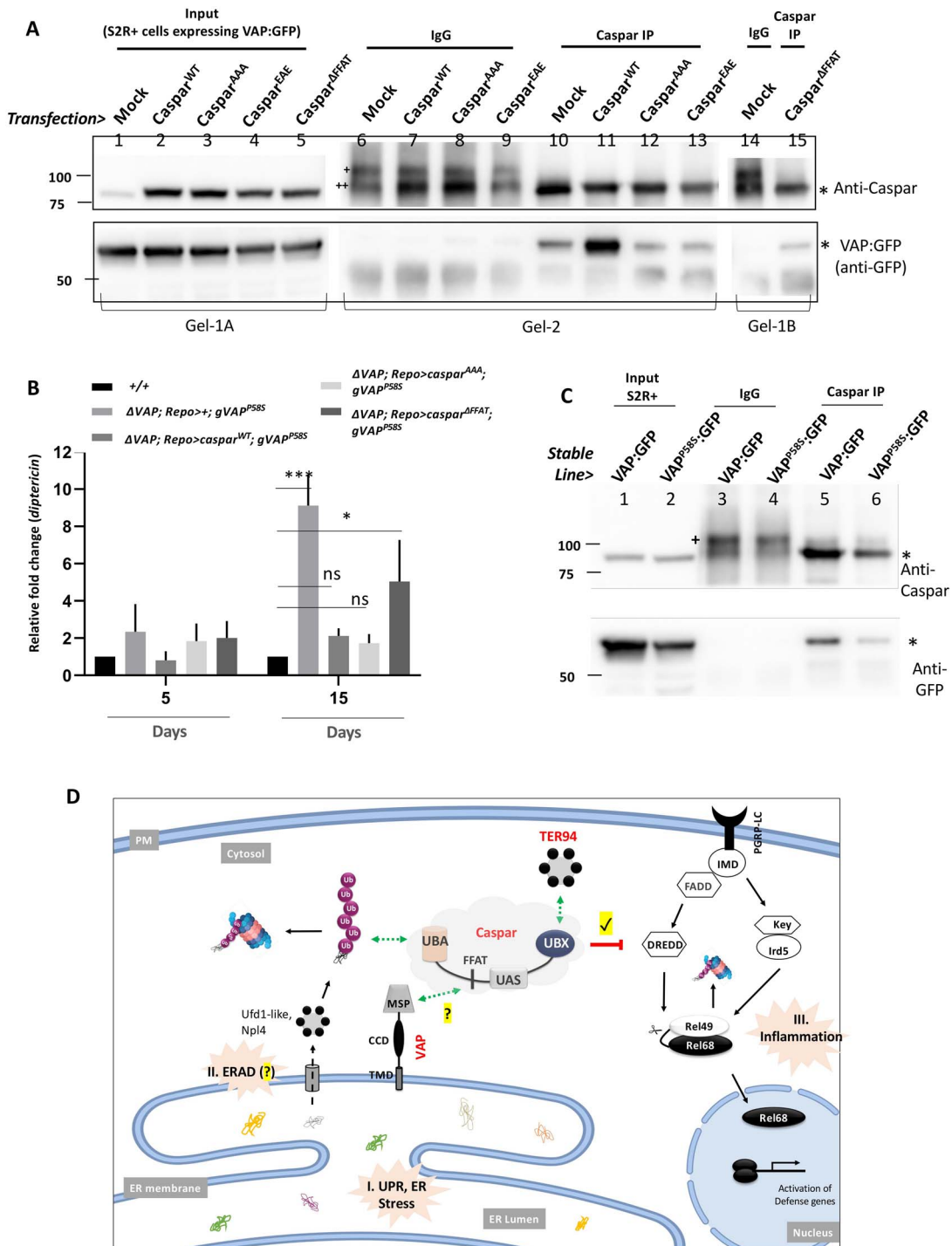


Figure 6. Caspar's ability to restrain age-dependent inflammation can delay the onset of disease, and this ability is independent of its interaction with VAP. **(A)** Mutations in the FFAT-like motif lead to disruption of the VAP:Caspar interaction. Caspar mutants were expressed in stable S2R+ lines expressing VAP:GFP. Affinity pull-downs using the anti-Caspar antibody could efficiently pull down VAP along with Caspar^{WT}. The antibody could, however, not pull down VAP efficiently in conditions when Caspar FFAT variants (AAA, EAE, Δ FFAT) were present. Protein bands that represent Caspar or VAP have been marked with a '*', whereas nonspecific bands are marked with either '+' or '++'. **(B)** Expression of the Rel target gene *dippterinin* in day-5 and day-15 adult heads of (i) wild-type (+/+), (ii) $\Delta VAP; Repo>+; gVAP^{P585}$, (iii) $\Delta VAP; Repo>caspar^{WT}; gVAP^{P585}$, (iv) $\Delta VAP; Repo>caspar^{AAA}; gVAP^{P585}$ and (v) $\Delta VAP; Repo>caspar^{\Delta FFAT}; gVAP^{P585}$ lines. The data suggest that FFAT-like mutants of Caspar do not interact with VAP and can yet suppress age-dependent inflammation. Values on the Y-axis depict the fold-change normalized to the housekeeping gene *rp49*. Values shown are mean \pm SEM. N = 3, n = 3. Statistical analysis by two-way ANOVA followed by Tukey's multiple comparison test. *P < 0.05, **P < 0.01, ***P < 0.001. **(C)** Caspar expresses natively in S2 cells. Affinity pull-down of VAP^{WT} and VAP^{P585} from independent stable S2R+ lines expressing VAP^{WT}:GFP and VAP^{P585}:GFP with the anti-Caspar antibody indicates that Caspar:VAP interaction is either at par or weaker when VAP^{P585} aggregates are present in the cell. Protein bands that represent Caspar or VAP have been marked with a '*', whereas nonspecific bands are marked with a '+' sign. **(D)** VAP^{P585} disease model depicting the players VAP, Caspar and TER94 in glial cells and their connectivity with IMD/Rel signalling, which regulates inflammation. The key features of the model include (i) ER stress caused directly or indirectly by VAP misfolding and (ii) a predicted upregulation of the protein degradation machinery in response to ER stress. VAP may act as a docking station, interacting with Caspar and TER94 to assist in proteasomal clearance. The AAA-ATPase TER94, itself an

patients. In the mouse model, cessation of NF κ B activity in microglia rescued motor neurons from early death and extended lifespan by reduction of inflammation. Glia has thus emerged as a cell type where NF κ B has critical roles in both vertebrates and invertebrates (82,83). *C9orf72*, a gene that is found to be perturbed in 60% of sALS patients appears to be required for proper macrophage and microglial function in mice (84). Also, NF κ B signalling appears to be activated in both fALS and sALS (85). NF- κ B, thus, appears to be an important signalling pathway in the glia (73,86).

Our study puts the spotlight on Caspar and its role in glial cells. On the basis of its domain structure (Fig. 6D) and our results, Caspar interacts with TER94, ubiquitinated proteins and has the ability to dock, via its FFAT-like motif onto the ER-resident VAP. As TER94 is orthologous to human VCP, which is itself an ALS locus, Caspar is unique in its ability to physically connect two orthologous ALS loci, ALS8 and ALS14 together, in flies. How important are these interactions and what is Caspar's functional role in our disease model? Our data rule out a role for glial Caspar as a mediator of clearance of VAP^{P58S} inclusions from the brain. On the positive side, the major role for Caspar in the glia appears to be its role in regulating inflammation of the brain, primarily by regulating Rel signalling. We also demonstrate, using Caspar variants that cannot bind to VAP, that Caspar does not need to be bound to VAP to negatively regulate Rel/NF κ B signalling. An important question that still remains is the molecular function of Caspar in the cell. On the basis of the available data, there are two possibilities; one, Caspar may be a facilitator of protein degradation of a few specific proteins involved in IMD/Rel signalling, which would include Dredd and Rel. The exact mechanism for regulation of Dredd by Caspar (52) has not been worked out and its degradative function may well be the answer. Two, Caspar may be an adapter that regulates the association of signalling complexes. For the second function, it may assist in capturing poly-Ub chains for modification of proteins in the signalosome. Activation via Ub-conjugation is a theme in the activation of the pathway (87,88). The Silverman and Meier laboratories have earlier documented mechanisms involved in K63-polyUb conjugation of IMD and Dredd by the E3-ligase DIAP2, along with the accessory proteins Effete, Bend and Uv1a, all of which are part of the complex (87,88). Unlike inflammation, other predicted functions of Caspar may depend on its physical interaction with VAP and these questions will need to be addressed in future studies.

Our model (Fig. 6D) that should parallel the onset and progression of disease in ALS incorporates the

three major physiological events that are central to glial homeostasis. First, animals expressing VAP^{P58S}, in the absence of wild-type VAP show ER stress (22,26,89,90) and morphological changes in the ER (91,92), a direct or indirect response to misfolded or partially folded mutant VAP proteins. The fact that VAP^{P58S} lines can progress through development, in the absence of VAP^{WT}, suggests that VAP^{P58S} is partially active, but this allelic variant is unable to sustain adult life beyond ~25 days. Second, the ER stress should lead to enhanced clearance by the UPS, with pathways such as ERAD (93), working overtime to maintain proteostasis. Our evidence for VAP and Caspar's involvement in proteasomal clearance (Fig. 6D) is indirect and primarily on the basis of its interaction with TER94 and the presence of ERAD components Ufd1-like and Npl4 in Caspar IPs. This in turn could lead to overload at the proteasome (94). Last, and directly on the basis of our data, the most important, there appears to be an age-dependent increase in glial inflammation in the disease model, which can be reined in by an increase in Caspar levels. This indirectly suggests that the Caspar pool available for suppressing Rel-mediated inflammation may be limited in the ALS8 model. Logically, the reason for this decrease would be the sequestration of Caspar, either by VAP^{P58S}, a phenomenon not ruled out by our data (Fig. 6C), or by diversion of Caspar to the overstrained proteasomal machinery (Fig. 6D).

In summary, we find that Caspar regulates age-dependent disease progression, primarily by regulating inflammation in glia. VAP appears to function as a docking site for Caspar; Caspar connects not only two ALS orthologous loci, namely VAP and TER94, together, it also links these to IMD/Rel signalling. Although functional roles for the Caspar:VAP interaction remain to be elucidated, Caspar appears to be an important point of convergence for critical cellular pathways that are central to motor neuron disease.

Materials and Methods

Drosophila husbandry, stocks and reagents

All flies were raised and crosses were conducted at 25°C in standard corn meal agar. The flies expressing genomic VAP^{WT} (*gVAP^{P58S} (VK31)/TM3TB*) and VAP^{P58S} (*gVAP^{WT} (VK31)/TM3TB*) were a kind gift from Hiroshi Tsuda (Moustaqim-Barrette et al., 2014). We balanced these with VAP Δ 166 to generate Δ 166/FM7A;+, *gVAP^{P58S} (VK31)/TM3TB and Δ 166/FM7A;+*; *gVAP^{WT} (VK31)/TM3TB*. The VAP Δ 166 allele was used instead of VAP Δ 31 used earlier because we were unsuccessful in receiving live VAP Δ 31 flies from the Tsuda laboratory. VAP Δ 166 (23),

ALS locus, may play an important role for this function. The clearance of VAP aggregates in the brain is not dependent on Caspar function in the glia, hence the '?' on the ERAD pathway. (iii) Age-dependent Inflammation, caused by misregulation of Rel signalling. Our data show that Caspar functions as a negative regulator for Rel signalling in glia (✓), and this function is attenuated in the disease. Mechanistically, this may be a consequence of a differential partitioning of the available glial Caspar pool for VAP or TER94-related functions. As the adult animal ages, a tipping point is reached when the increasing burden of ER stress, proteasomal overload and glial inflammation leads to motor neuron cell death, subsequently followed by the death of the organism. The VAP:Caspar interaction itself (↔), via the Caspar FFAT motif appears not to be required (?) for Caspar to regulate glial inflammation. Double-headed arrows indicate interactions between proteins, whereas single headed arrows (→) indicate key cellular pathways.

like the *VAP Δ 31* allele, is a larval/pupal lethal. The primary lines used for our experiments, Δ 166;+;gVAP^{WT} and Δ 166;+;gVAP^{P585} are at par with the Tsuda lines in terms of lifespan, cytoplasmic VAP inclusions and motor dysfunction.

Further, these lines were modified by adding Gal4 driver chromosomes for the second chromosome. The Gal4 drivers used were *MHC-Gal4*, *OK6-Gal4* and *Repo-Gal4*.

The UAS-VAP^{WT} and UAS-VAP^{P585} were generated in the Jackson laboratory (36). Lines procured from the Bloomington *Drosophila* Stock Centre are as follows: name (Stock #), Canton-S (0001), UAS-VAP^{RNAi} (27312), UAS-TBPH^{RNAi} (29517), UAS-caz^{WT} (17010), UAS-caz^{RNAi} (34839), UAS-SOD^{WT} (24754), UAS-SOD1^{RNAi} (34616), UAS-TER94^{RNAi} (32869), UAS-alsin^{WT} (27162), UAS-alsin^{RNAi} (28533), UAS-senataxin^{RNAi} (34683), *MHC-Gal4* (38464), *OK-Gal4* (64199), UAS-caspar^{RNAi} (44027), UAS-Rel^{RNAi} (33661), UAS-Rel^{WT} (9459), *Relish^{E20}* (55714), UAS-Imd^{RNAi} (38933), UAS-ird5^{WT} (90312), UAS-ird5^{RNAi} (57751), UAS-Dredd^{RNAi} (34070), UAS-PGRP-LE^{RNAi} (60038), UAS-PGRP-LC^{WT} (30919), UAS-caspar^{RNAi} (44027), *caspar^{lof}* (11373) and *caspar* deficiency (23691). Lines procured from the National Institute of Genetics were UAS-Rel^{11992R-1} and UAS-Rel^{11992R-2}. The UAS-TBPH:FLAG:HA^{WT} line was procured from the National Centre for Biological Sciences Stock Centre (NCBS, 95), whereas UAS-TER94^{WT}, UAS-TER94^{R152H} and UAS-TER94^{A229E} were procured from the Taylor laboratory (45). Third chromosome *apterous-Gal4* and *daughterless Gal4* were procured from the Shashidhara laboratory. The second chromosome *Repo-Gal4* (96) was a kind gift from Dr Bradley Jones. UAS-*caspar*:HA was generated by procuring the cloned vector UFO05904 from the *Drosophila* Genomics Resource Centre tagged-ORF collection and generating transgenic animals at the NCBS transgenic facility. Expression of the line was validated by monitoring transcripts by real-time PCR and protein expression by anti-HA and anti-Caspar antibodies. The *caspar^{lof}* (*casp^{C04227}*) line is a gypsy insert in the *caspar* locus and is a strong hypomorphic (near-null) allele (Supplementary Material, Fig. S2A).

Cloning and expression of Caspar^{EAE}, Caspar^{AAA} and Caspar^{AFFAT}

Caspar FFAT-like mutants, generated for the purpose of S2 cell culture were subcloned into pRM vectors (97), with a N-terminal Myc tag and subsequently sequenced to confirm the mutations. For the Δ FFAT construct, 21 nucleotides were deleted from the region coding for the FFAT-like motif 'EFEDATD'. UAS-Caspar constructs were generated starting with the pUASp-attB-Caspar construct, with the design including an N-terminal HA tag, and constructs sequenced for before injecting in w¹¹¹⁸ embryos. Caspar expression in the stable, transgenic fly lines was validated using western blots. Primer pairs used for pRM cloning were as follows: forward and reverse primers, respectively, for Caspar^{EAE} mutant: CAGATGCCGCCGCGATGCCACAGACTTCAACAACGCC

and CATCGGCGCGGCATCTGTGCGAGCTCTCACTGTCC; Caspar^{AAA} mutant GAGCTCGACAGATGAGGCCGAAGATGCCACAGACTTC and GAAGTCTGTGGCATCTTCGGCCTCATCTGTGCGAGCTCTC; Caspar^{AFFAT} mutant GAGCTCGACAGATTTCAACAACGCCGAGTACATATTTACTGAC and CGTTGTTGAAATCTGTGCGAGCTCTCACTGTCCAC.

For cloning in pUASP-attB, primers used are as follows: primer with HA overhang, ATAGCCACTAGTGATCTGATGTACCCATACGATGTTCCAGATTACGCTGGCGC; *caspar* (forward) GTCAGAGAACAAGGACGAGGC, GGAACGGTCATCCTGGAGGAG and GCAGCTGGGCACTCGTTATG; *caspar* (reverse) CCTGCGGATACAGCTTGAGC, CTCTCCAGGATGACCGTTTCC, GGCCTCGTCCTTGTCTCTGAC & GCCGTGATGCAAGTAAATGGCC.

Lifespan and survival analysis

Survival assays were carried out on the genomic VAP (gVAP) lines (Fig. 1A) and their derivatives (Supplementary Material, Fig. S1; Fig. 1D). For each experiment, ~100 F1 male flies of the desired genotype were collected with each vial containing 15 or less age-matched flies. Animals were flipped to a fresh vial every fourth day, with number of flies recorded per vial on a daily basis, till all flies, including those in control experiments were dead. The survival data were plotted and analyzed using the log-rank test in Prism 7, which compares the entire survival curve(s) and gives a value of significance as a P-value, which was recorded and reported as a colour-coded map (Fig. 1D). The ML for each curve was also calculated and used as a simple readout for each experiment.

Generation of Caspar antibody

Full-length *caspar* was sub-cloned into pET-45b. The N-terminal 6 \times -His-Tagged Caspar was expressed in *Escherichia coli* BL21DE3 cells. In total, 1 mM Isopropyl β -D-1-thiogalactopyranoside was used to induce expression of protein at 25°C. The cellular lysate, in 1 \times Tris-Buffer Saline (TBS), 10 mM Imidazole was incubated with Ni-NTA beads (Qiagen) and the bound protein of interest was eluted using increasing concentrations of Imidazole, namely, 25, 50, 100 and 150 mM. Caspar eluted at both 50 and 100 mM. The fractions were merged, concentrated and injected into a GE Healthcare Sephadex-G200 preparative column. Fractions of the major peak at 150 kDa were collected and the eluted protein showed a molecular weight of 66 kDa in SDS-PAGE gels, suggesting that Caspar was a dimer in its native state. The column-purified protein was used to generate a Rabbit Polyclonal antibody by Bioklone (Chennai, India). The serum was further purified with Caspar conjugated to Protein A beads and the Caspar-enriched IgG used for further experiments. The antibody was validated (Supplementary Material, Fig. S2). The working dilutions for the antibody were 1:20 000 for western blots and 1:1000 for tissue.

IP, western blot analysis

In total, 5- to 10-day-old adult flies were lysed in Co-IP Lysis Buffer (20 mM Tris pH 8.0, 137 mM NaCl, 1% IGEPAL, 2 mM EDTA, 1× PIC) using a Dounce homogenizer and centrifuged at 21000g for 30 min. S2 cells transfected with the pRM Caspar constructs for 48 h were lysed with the Co-IP Lysis Buffer and cleared by centrifugation at 21000g for 30 min. 3 mg of total fly lysate or 1 mg of the S2 cell lysate was incubated with 5 μg of primary antibody (Rb anti-Caspar or Rb anti-VAP) and 5 μg of Normal Rabbit IgG overnight at 4°C. The Anti-VAP antibody was generated as described (30,37). Antigen-antibody complexes were captured using 50 μl of BioRad SureBeads Protein A (1614013) at 4°C for 4 h. Beads were washed six times with Co-IP lysis buffer and protein complexes eluted by boiling in 1× Laemmli sample buffer. Eluted proteins were resolved on a 10% polyacrylamide gel followed by western blotting or in-gel trypsin digestion. Proteins separated by SDS-PAGE were transferred onto a PVDF membrane (Immobilon-E, Merck) and blocked in 5% milk in TBS with 0.1% Tween 20 (TBS-T) for an hour. Blots were then incubated overnight with primary antibody diluted in 5% milk in TBS-T, at 4°C. Following three washes with TBS-T, blots were incubated with secondary antibodies diluted in 5% milk in TBS-T, for 1 h at RT. Blots were washed thrice with TBS-T and visualized on a LAS4000 Fuji imaging system after incubating with Immobilon Western Chemiluminescent HRP substrate (Merck). The following antibodies were used: Rabbit anti-VAP, 1:10 000 (30,37); Mouse anti- α -Tubulin, 1:10 000 (T6074, Sigma-Aldrich); Rabbit anti-VCP, 1:1000 (2648, Cell Signaling Technology); Mouse anti-GFP, 1:5000 (11814460001, Roche); Goat anti-rabbit HRP and Goat anti-mouse HRP secondary antibodies, each at 1:10 000 (Jackson ImmunoResearch).

In-gel trypsin digestion and LC-MS/MS analysis

Before in-gel trypsin digestion of the Co-IP eluate, the antibody was crosslinked to the SureBeads using DMP (Sigma) according to the NEB crosslinking protocol to avoid elution of the antibody. After crosslinking 10 μg Caspar antibody, Co-IP was performed as described above. In-gel trypsin digestion was carried out as previously described (98). Briefly, Coomassie-stained bands on the gel were excised and cut into 1 mm cubes. Gel pieces were transferred to a clean microcentrifuge tube and destained with buffer containing 50% acetonitrile in 50 mM Ammonium bicarbonate. Reduction and alkylation were carried out on the destained gel pieces by incubating with 10 mM dithiothreitol followed by incubating with 20 mM iodoacetamide. Gel pieces were saturated with sequencing grade Trypsin (Promega) at a concentration of 10 ng/μl and incubated overnight at 37°C. Peptides were extracted by sequential addition of 100 μl of 0.4% Trifluoroacetic acid (TFA) in 10% ACN, 100 μl of 0.4% TFA in 60% ACN and 100 μl of ACN. The pooled extract was dried in a vacuum centrifuge and

reconstituted with 50 μl of 0.1% TFA. The peptides in TFA were purified using the StageTip protocol (99).

LC-MS/MS analysis was performed on the Sciex TripleTOF6600 mass spectrometer interfaced with an Eksigent nano-LC 425. Tryptic peptides (1 μg) were loaded onto an Eksigent C18 trap (5 μg capacity) and subsequently eluted with a linear acetonitrile gradient on an Eksigent C18 analytical column (15 cm × 75 μm internal diameter). A typical LC run lasted 2 h post loading onto the trap at a constant flow rate of 300 nl/min with solvent A consisting of water + 0.1% formic acid and solvent B consisting of acetonitrile. The gradient schedule for the LC run was 5% (vol/vol) B for 10 min, a linear gradient of B from 0% to 80% (vol/vol) over 80 min, 80% (vol/vol) B for 15 min and equilibration with 5% (vol/vol) B for 15 min. Data were acquired in an information-dependent acquisition mode over a mass range of 300–2000 m/z. Each full MS survey scan was followed by MS/MS of the 15 most intense peptides. Dynamic exclusion was enabled for all experiments (repeat count 1; exclusion duration 6 s). Peptide identification and quantification were carried out with the SCIEX ProteinPilot software at a false discovery rate of 1%. A RefSeq *Drosophila* protein database (release 6) was used for peptide identification. Proteins that were identified in two or more replicates and had two or more quantified peptides were tabulated.

Motor function

Motor performance of each genotype was analyzed using the standard startle induced negative geotaxis climbing assay (100,101), with minor modifications. Three separate sets (biological replicates) of 30 age-matched adult males of each genotype were raised at 25°C, with 15 males in each vial. Each experimental set of 30 flies was transferred in a 250 ml (30 cm) glass cylinder and allowed to acclimatize for around 5 min. These flies were then tapped to induce a startle and were allowed to climb for 60 s. After 60 s, the flies were scored into three kinds on the basis of their position in the cylinder. Flies that did not climb were scored 0 (Non-Climbers), flies that climbed till 80 ml (7.5 cm) mark were scored 1 (Bad Climbers) and flies that climbed beyond 80 ml were scored 2 (Good Climbers). This was repeated thrice for each set of flies. A 3 min resting window was used in between the trials for each genotype. The climbing assays were conducted for a genotype every 5 days till at least one genotype completely stopped climbing or the flies were dead. The flies were exposed to CO₂ only after a day's trial was complete, ensuring no effect of anaesthesia on the assay. Flies were transferred to a fresh vial every 4 days to avoid death because of sticky media. The scores were used to calculate the climbing index of replicates. Statistical analysis was performed using two-way analysis of variance (ANOVA) followed by multiple comparison testing by Tukey's test. The climbing index is a proxy for the fitness of a particular fly/genotype on a particular day and can be used as a readout for

any progression of the motor defect in a set of flies. The climbing index was calculated as described in (102).

Microscopy, staining and image analysis

For larval brains, wandering third instar larvae were selected and the brains dissected in phosphate buffer saline (1× PBS). Fixation was carried out in 4% PFA with 0.3% Triton-X in PBS for 20 min followed by three washes with 1× PBS. The brains were blocked in 2% BSA with 0.3% Triton X-100 in PBS for 1.5 h and then incubated in primary antibodies overnight at 4°C. This was followed by 1.5 h wash with blocking solution and incubation in Alexa Fluor secondary antibodies for 1.5 h at room temperature, followed by four 20 min washes with the blocking solution. DAPI (4,6 diamidino-2-phenylindole DAPI) was added during the second wash (1:1000). Samples were then washed with PBS, mounted in 70% glycerol with n-propyl gallate and the areas of the ventral nerve cord were imaged under Zeiss Confocal microscopes at 63× oil magnification. Antibodies utilized are as follows: M Anti-Repo (DSHB; 1:100), Rat Anti-ELAV (DSHB; 1:100) and Rb Anti-VAP (30,37). The analysis was as described earlier (30).

For the adult brain preparations, flies were anaesthetized using CO₂ and their brains dissected in 1× PBS (pH 7.4). The brains were fixed in 1.2% PFA for 24 h at 4°C, then washed twice in 5% PBST for 20 min, followed by two 30 min washes in PAT (0.5% BSA with 0.5% Triton X-100 in 1× PBS) buffer. The samples were then blocked in 5% BSA for 2 h. The brains were incubated in primary antibody for 36 h at 4°C then washed in PAT Buffer, followed by incubation with secondary antibody for another 36 h. The samples were washed four times in PAT buffer, 1 h each wash. DAPI was added during the second wash. Next, samples were washed with PBS, mounted in Slowfade mounting medium (Vectashield, S36937) and imaged. Images were acquired on a Leica Sp8, using a 63× objective with a zoom factor of 0.75. Z stacks were acquired with an interval of 1 μm at 16-bit depth. Images were analyzed by Huygens Professional software (HuPro CE 18.10.0p2) from Scientific Volume Imaging, as described (30), with modifications. 5–10 brains were analyzed per experiment with five regions of interest (ROIs) per brain. The ROIs were chosen in the sub-oesophageal region of the brain. Parameters measured were ‘aggregate volume’ in μm³ and ‘aggregate density’ as the number of aggregates per μm³. Data were represented as normalized values to the control (Δ VAP;Repo>+; gVAP^{P585}) on each day (Fig. 4J–O). Graphpad prism 7 was used to plot the data. For statistical analysis, one-way ANOVA was used followed by Tukey’s multiple comparison test statistical significance.

Real-time PCR

mRNA was extracted from 50 to 80 adult heads (5- and 15-day-old) using the Qiagen RNAeasy mini kit (74104). A total of 1 μg of mRNA was used for the cDNA synthesis using the High Capacity cDNA Reverse

Transcriptase Kit (4368814) by Applied Biosystems. The qPCR was carried out using KAPA SYBR FAST (KK4602) by Sigma using Eppendorf Realplex Mastercycler. The experiments were carried out thrice with three technical replicates each. The relative fold-change for each genotype was calculated by normalizing to the housekeeping gene *rp49*. The data were analyzed using two-way ANOVA followed by Tukey’s test for multiple comparison. Primers pairs used (60,97) were as follows: *rp49 Forward(-f)*: GACGCTTCAAGGGACAGTATC, *rp49 reverse(-r)*: AAACGCGGTTCTGCATGAG; *attacinD-f*: CGGTCAACGCCAATGGTCAT, *attacinD-r*: CATTACAGAGCGGCGT-TATTG; *diptericein-f*: ACCGCAGTACCCACTCAATC, *diptericein-r*: GGTCCACACCTTCTGGTGAC; *cecropinA1-f*: CATTGGA-CAATCGGAAGCTGGGTG, *cecropinA1-r*: TAATCATCGTG-GTCAACCTCGGGC; *drosocin-f*: GTTCACCATCGTTTTCC, *drosocin-r*: CCACACCCATGGCAAAAAC; *metchnikowin-f*: GCTACATCAGTGCTGGCAGA, *metchnikowin-r*: AATAAATTG-GACCCGGTCT.

Supplementary Material

Supplementary Material is available at HMG online.

Author Contributions

S.T. and G.R. conceptualized the project. S.T., S.H., A.T., L.G. and B.K. executed the experiments, collected data and analyzed the same. A.R. and G.R. were involved in supervision, project administration and funding acquisition. All authors contributed to the writing and editing of manuscript.

Acknowledgements

We thank BDSC, supported by NIH grant P40OD018537, for fly stocks; FlyBase, supported by a grant from the National Human Genome Research Institute at the U.S. National Institutes of Health U41HG000739; National Institute Genetics (NIG), Japan, for fly stocks; *Drosophila* Genome Resource Centre (DGRC), supported by NIH grant 2P40OD010949, for vectors and clones; Transgenic RNAi project (TRiP), at the Harvard Medical School supported by NIH/NIGMS R01-GM084947, for providing transgenic RNAi fly stocks; Transgenic injection facility at the National Centre for Biological Sciences (NCBS); Indian Institute of Science Education and Research (IISER) Imaging Facility for access to microscopy and analysis resources; IISER Proteomics facility for training of students and access to instruments; Neel Wagh for technical support.

Conflict of Interest statement. None declared.

Funding

Indian Council for Medical Research (ICMR) (#2020-4887); Department of Biotechnology (DBT), Govt. of India (grant

#BT/PR26095/GET/119/199/2017); Science and Engineering Board (SERB), Department of Science and Technology, Govt. of India (grant #CRG/2018/001218); National Facility for Gene Function in Health and Disease (NFGFHD) (DBT grant BT/INF/22/SP17358/2016); Agharkar Research Institute, Pune (to A.R.); Indian Institute of Science Education and Research, Pune (to G.S.R.); IISER Fellowships (to S.T., A.T. and L.G.); Council for Scientific and Industrial Research (CSIR), Govt. of India (to S.H.).

References

- Mitchell, J.D. and Borasio, G.D. (2007) Amyotrophic lateral sclerosis. *Lancet*, **369**, 2031–2041.
- Pasinelli, P. and Brown, R.H. (2006) Molecular biology of amyotrophic lateral sclerosis: insights from genetics. *Nat. Rev. Neurosci.*, **7**, 710–723.
- Cleveland, D.W. and Rothstein, J.D. (2001) From Charcot to Lou Gehrig: deciphering selective motor neuron death in ALS. *Nat. Rev. Neurosci.*, **2**, 806–819.
- Deng, H.X., Hentati, A., Tainer, J.A., Iqbal, Z., Cayabyab, A., Hung, W.Y., Getzoff, E.D., Hu, P., Herzfeldt, B., Roos, R.P. et al. (1993) Amyotrophic lateral sclerosis and structural defects in Cu,Zn superoxide dismutase. *Science*, **261**, 1047–1051.
- Rosen, D.R., Siddique, T., Patterson, D., Figlewicz, D.A., Sapp, P., Hentati, A., Donaldson, D., Goto, J., O'Regan, J.P., Deng, H.-X. et al. (1993) Mutations in cu/Zn superoxide dismutase gene are associated with familial amyotrophic lateral sclerosis. *Nature*, **362**, 59–62.
- Abel, O., Powell, J.F., Andersen, P.M. and Al-Chalabi, A. (2012) ALSod: a user-friendly online bioinformatics tool for amyotrophic lateral sclerosis genetics. *Hum. Mutat.*, **33**, 1345–1351.
- Robberecht, W. and Philips, T. (2013) The changing scene of amyotrophic lateral sclerosis. *Nat. Rev. Neurosci.*, **14**, 248–264.
- Chance, P.F., Rabin, B.A., Ryan, S.G., Ding, Y., Scavina, M., Conway, D., Crain, B., Griffin, J.W. and Cornblath, D.R. (1998) Linkage of the gene for an autosomal dominant form of juvenile amyotrophic lateral sclerosis to chromosome 9q34. *Am. J. Hum. Genet.*, **62**, 633–640.
- Vance, C., Rogelj, B., Hortobagyi, T., De Vos, K.J., Nishimura, A.L., Sreedharan, J., Hu, X., Smith, B., Ruddy, D., Wright, P. et al. (2009) Mutations in FUS, an RNA processing protein, cause familial amyotrophic lateral sclerosis type 6. *Science*, **323**, 1208–1211.
- Nishimura, A.L., Mitne-Neto, M., Silva, H.C.A., Richieri-Costa, A., Middleton, S., Cascio, D., Kok, F., Oliveira, J.R.M., Gillingwater, T., Webb, J. et al. (2004) A mutation in the vesicle-trafficking protein VAPB causes late-onset spinal muscular atrophy and amyotrophic lateral sclerosis. *Am. J. Hum. Genet.*, **75**, 822–831.
- Nicolas, A., Kenna, K.P., Renton, A.E., Ticozzi, N., Faghri, F., Chia, R., Dominov, J.A., Kenna, B.J., Nalls, M.A., Keagle, P. et al. (2018) Genome-wide analyses identify KIF5A as a novel ALS gene. *Neuron*, **97**, 1268–1283.
- van Blitterswijk, M., van Es, M.A., Hennekam, E.A., Dooijes, D., van Rheenen, W., Medic, J., Bourque, P.R., Schelhaas, H.J., van der Kooi, A.J., de Visser, M. et al. (2012) Evidence for an oligogenic basis of amyotrophic lateral sclerosis. *Hum. Mol. Genet.*, **21**, 3776–3784.
- Leblond, C.S., Kaneb, H.M., Dion, P.A. and Rouleau, G.A. (2014) Dissection of genetic factors associated with amyotrophic lateral sclerosis. *Exp. Neurol.*, **262**, 91–101.
- Renton, A.E., Chio, A. and Traynor, B.J. (2014) State of play in amyotrophic lateral sclerosis genetics. *Nat. Neurosci.*, **17**, 17–23.
- Murphy, S.E. and Levine, T.P. (2016) VAP, a versatile access point for the endoplasmic reticulum: review and analysis of FFAT-like motifs in the VAPome. *Biochim. Biophys. Acta*, **1861**, 952–961.
- Lev, S., Ben Halevy, D., Peretti, D. and Dahan, N. (2008) The VAP protein family: from cellular functions to motor neuron disease. *Trends Cell Biol.*, **18**, 282–290.
- Kamemura, K. and Chihara, T. (2019) Multiple functions of the ER-resident VAP and its extracellular role in neural development and disease. *J. Biochem.*, **165**, 391–400.
- Cabukusta, B., Berlin, I., van Elsland, D.M., Forkink, I., Spits, M., de Jong, A.W.M., Akkermans, J.J.L.L., Wijdeven, R.H.M., Janssen, G.M.C., van Veelen, P.A. et al. (2020) Human VAPome analysis reveals MOSPD1 and MOSPD3 as membrane contact site proteins interacting with FFAT-related FFNT motifs. *Cell Rep.*, **33**, 108475. doi: 10.1016/j.celrep.2020.108475.
- Di Mattia, T., Martinet, A., Ikhlef, S., McEwen, A.G., Nomine, Y., Wendling, C., Poussin-Courmontagne, P., Voilquin, L., Eberling, P., Ruffenach, F. et al. (2020) FFAT motif phosphorylation controls formation and lipid transfer function of inter-organelle contacts. *EMBO J.*, **39**, e104369.
- Lindhout, F.W., Cao, Y.J., Kevenaar, J.T., Bodzeta, A., Stucchi, R., Boumpoutsari, M.M., Katrukha, E.A., Altelaar, M., MacGillivray, H.D. and Hoogenraad, C.C. (2019) VAP-SCRN1 interaction regulates dynamic endoplasmic reticulum remodeling and presynaptic function. *EMBO J.*, **38**, e101345.
- Mao, D.X., Lin, G., Tepe, B., Zuo, Z.Y., Li Tan, K., Senturk, M., Zhang, S., Arenkiel, B.R., Sardiello, M. and Bellen, H.J. (2019) VAMP associated proteins are required for autophagic and lysosomal degradation by promoting a PtdIns4P-mediated endosomal pathway. *Autophagy*, **15**, 1214–1233.
- Moustaqim-Barrette, A., Lin, Y.Q., Pradhan, S., Neely, G.G., Bellen, H.J. and Tsuda, H. (2014) The amyotrophic lateral sclerosis 8 protein, VAP, is required for ER protein quality control. *Hum. Mol. Genet.*, **23**, 1975–1989.
- Pennetta, G., Hiesinger, P.R., Fabian-Fine, R., Meinertzhagen, I.A. and Bellen, H.J. (2002) *Drosophila* VAP-33A directs Bouton formation at neuromuscular junctions in a dosage-dependent manner. *Neuron*, **35**, 291–306.
- Han, S.M., Tsuda, H., Yang, Y., Vibbert, J., Cottee, P., Lee, S.J., Winek, J., Haueter, C., Bellen, H.J. and Miller, M.A. (2012) Secreted VAPB/ALS8 major sperm protein domains modulate mitochondrial localization and morphology via growth cone guidance receptors. *Dev. Cell*, **22**, 348–362.
- Tsuda, H., Han, S.M., Yang, Y., Tong, C., Lin, Y.Q., Mohan, K., Haueter, C., Zoghbi, A., Harati, Y., Kwan, J. et al. (2008) The amyotrophic lateral sclerosis 8 protein VAPB is cleaved, secreted, and acts as a ligand for Eph receptors. *Cell*, **133**, 963–977.
- Larroquette, F., Seto, L., Gaub, P.L., Kamal, B., Wallis, D., Lariviere, R., Vallee, J., Robitaille, R. and Tsuda, H. (2015) Vap-b/amyotrophic lateral sclerosis 8 knock-in mice display slowly progressive motor behavior defects accompanying ER stress and autophagic response. *Hum. Mol. Genet.*, **24**, 6515–6529.
- Teuling, E., Ahmed, S., Haasdijk, E., Demmers, J., Steinmetz, M.O., Akhmanova, A., Jaarsma, D. and Hoogenraad, C.C. (2007) Motor neuron disease-associated mutant vesicle-associated membrane protein-associated protein (VAP) B recruits wild-type VAPs into endoplasmic reticulum-derived tubular aggregates. *J. Neurosci.*, **27**, 9801–9815.
- Borgese, N., Iacomino, N., Colombo, S.F. and Navone, F. (2021) The link between VAPB loss of function and amyotrophic lateral sclerosis. *Cell*, **10**, 1865.
- Deivasigamani, S., Verma, H.K., Ueda, R., Ratnaparkhi, A. and Ratnaparkhi, G.S. (2014) A genetic screen identifies tor as an

- interactor of VAPB in a *Drosophila* model of amyotrophic lateral sclerosis. *Biol. Open*, **3**, 1127–1138.
30. Chaplot, K., Pimpale, L., Ramalingam, B., Deivasigamani, S., Kamat, S.S. and Ratnaparkhi, G.S. (2019) SOD1 activity threshold and TOR signalling modulate VAP(P58S) aggregation via reactive oxygen species-induced proteasomal degradation in a *Drosophila* model of amyotrophic lateral sclerosis. *Dis. Model. Mech.*, **12**, dmm033803.
 31. Chu, K.T., Niu, X.H. and Williams, L.T. (1995) A Fas-associated protein factor, Faf1, potentiates Fas-mediated apoptosis. *Proc. Natl. Acad. Sci. U.S.A.*, **92**, 11894–11898.
 32. Ryu, S.W., Lee, S.J., Park, M.Y., Jun, J., Jung, Y.K. and Kim, E. (2003) Fas-associated factor 1, FAF1, is a member of Fas death-inducing signaling complex. *J. Biol. Chem.*, **278**, 24003–24010.
 33. Kang, W. and Yang, J.K. (2011) Crystal structure of human FAF1 UBX domain reveals a novel Fcisp touch-turn motif in p97/VCP-binding region. *Biochem. Biophys. Res. Commun.*, **407**, 531–534.
 34. Kim, K.H., Kang, W., Suh, S.W. and Yang, J.K. (2011) Crystal structure of FAF1 UBX domain in complex with p97/VCP N domain reveals a conformational change in the conserved Fcisp touch-turn motif of UBX domain. *Proteins*, **79**, 2583–2587.
 35. Baron, Y., Pedrioli, P.G., Tyagi, K., Johnson, C., Wood, N.T., Fontaine, D., Wightman, M. and Alexandru, G. (2014) VAPB/ALS8 interacts with FFAT-like proteins including the p97 cofactor FAF1 and the ASNA1 ATPase. *BMC Biol.*, **12**, 39.
 36. Ratnaparkhi, A., Lawless, G.M., Schweizer, F.E., Golshani, P. and Jackson, G.R. (2008) A *Drosophila* model of ALS: human ALS-associated mutation in VAP33A suggests a dominant negative mechanism. *PLoS One*, **3**, e2334.
 37. Yadav, S., Thakur, R., Georgiev, P., Deivasigamani, S., Krishnan, H., Ratnaparkhi, G. and Raghu, P. (2018) RDGBalpha localization and function at membrane contact sites is regulated by FFAT-VAP interactions. *J. Cell Sci.*, **131**, jcs207985.
 38. Chai, A., Withers, J., Koh, Y.H., Parry, K., Bao, H., Zhang, B., Budnik, V. and Pennetta, G. (2008) hVAPB, the causative gene of a heterogeneous group of motor neuron diseases in humans, is functionally interchangeable with its *Drosophila* homologue DVAP-33A at the neuromuscular junction. *Hum. Mol. Genet.*, **17**, 266–280.
 39. Forrest, S., Chai, A., Sanhueza, M., Marescotti, M., Parry, K., Georgiev, A., Sahota, V., Mendez-Castro, R. and Pennetta, G. (2013) Increased levels of phosphoinositides cause neurodegeneration in a *Drosophila* model of amyotrophic lateral sclerosis. *Hum. Mol. Genet.*, **22**, 2689–2704.
 40. Sanhueza, M., Chai, A., Smith, C., McCray, B.A., Simpson, T.I., Taylor, J.P. and Pennetta, G. (2015) Network analyses reveal novel aspects of ALS pathogenesis. *PLoS Genet.*, **11**, e1005107.
 41. Boillee, S., Vande Velde, C. and Cleveland, D.W. (2006) ALS: a disease of motor neurons and their nonneuronal neighbors. *Neuron*, **52**, 39–59.
 42. Loewen, C.J. and Levine, T.P. (2005) A highly conserved binding site in vesicle-associated membrane protein-associated protein (VAP) for the FFAT motif of lipid-binding proteins. *J. Biol. Chem.*, **280**, 14097–14104.
 43. Loewen, C.J., Roy, A. and Levine, T.P. (2003) A conserved ER targeting motif in three families of lipid binding proteins and in Opi1p binds VAP. *EMBO J.*, **22**, 2025–2035.
 44. Chang, Y.C., Hung, W.T., Chang, Y.C., Chang, H.C., Wu, C.L., Chiang, A.S., Jackson, G.R. and Sang, T.K. (2011) Pathogenic VCP/TER94 alleles are dominant actives and contribute to neurodegeneration by altering cellular ATP level in a *Drosophila* IBMPPFD model. *PLoS Genet.*, **7**, e1001288.
 45. Ritson, G.P., Custer, S.K., Freibaum, B.D., Guinto, J.B., Geffel, D., Moore, J., Tang, W.X., Winton, M.J., Neumann, M., Trojanowski, J.Q. et al. (2010) TDP-43 mediates degeneration in a novel *Drosophila* model of disease caused by mutations in VCP/p97. *J. Neurosci.*, **30**, 7729–7739.
 46. Zhang, X.Y., Gui, L., Zhang, X.Y., Bulfer, S.L., Sanghez, V., Wong, D.E., Lee, Y., Lehmann, L., Lee, J.S., Shih, P.Y. et al. (2015) Altered cofactor regulation with disease-associated p97/VCP mutations. *Proc. Natl. Acad. Sci. U.S.A.*, **112**, E1705–E1714.
 47. van den Boom, J. and Meyer, H. (2018) VCP/p97-mediated unfolding as a principle in protein homeostasis and signaling. *Mol. Cell*, **69**, 182–194.
 48. Yeung, H.O., Kloppsteck, P., Niwa, H., Isaacson, R.L., Matthews, S., Zhang, X.D. and Freemont, P.S. (2008) Insights into adaptor binding to the AAA protein p97. *Biochem. Soc. Trans.*, **36**, 62–67.
 49. Ruggiano, A., Foresti, O. and Carvalho, P. (2014) ER-associated degradation: protein quality control and beyond. *J. Cell Biol.*, **204**, 868–878.
 50. Frakes, A.E. and Dillin, A. (2017) The UPRER: sensor and coordinator of organismal homeostasis. *Mol. Cell*, **66**, 761–771.
 51. Ernst, W.L., Shome, K., Wu, C.C., Gong, X., Frizzell, R.A. and Aridor, M. (2016) VAMP-associated proteins (VAP) as receptors that couple cystic fibrosis transmembrane conductance regulator (CFTR) proteostasis with lipid homeostasis. *J. Biol. Chem.*, **291**, 5206–5220.
 52. Kim, M., Lee, J.H., Lee, S.Y., Kim, E. and Chung, J. (2006) Caspar, a suppressor of antibacterial immunity in *Drosophila*. *Proc. Natl. Acad. Sci. U.S.A.*, **103**, 16358–16363.
 53. Leulier, F., Rodriguez, A., Khush, R.S., Abrams, J.M. and Lemaitre, B. (2000) The *Drosophila* caspase Dredd is required to resist gram-negative bacterial infection. *EMBO Rep.*, **1**, 353–358.
 54. Stoven, S., Ando, I., Kadalayil, L., Engstrom, Y. and Hultmark, D. (2000) Activation of the *Drosophila* NF-kappa B factor relish by rapid endoproteolytic cleavage. *EMBO Rep.*, **1**, 347–352.
 55. Menges, C.W., Altomare, D.A. and Testa, J.R. (2009) FAS-associated factor 1 (FAF1) diverse functions and implications for oncogenesis. *Cell Cycle*, **8**, 2528–2534.
 56. Min-Young, P., Ji-Hyun, M. and Eunhee, K. (2004) Fas associated factor 1, FAF1, impairs NF-kappaB activation by interacting with the I kappa B kinase complex. *Mol. Biol. Cell*, **15**, 2544–2549.
 57. Park, M.Y., Moon, J.H., Lee, K.S., Choi, H.I., Chung, J., Hong, H.J. and Kim, E. (2007) FAF1 suppresses I kappa B kinase (IKK) activation by disrupting the IKK complex assembly. *J. Biol. Chem.*, **282**, 27572–27577.
 58. Chen, P., Rodriguez, A., Erskine, R., Thach, T. and Abrams, J.M. (1998) DREDD, a novel effector of the apoptosis activators REAPER, GRIM, and HID in *Drosophila*. *Dev. Biol.*, **201**, 202–216.
 59. Hu, S.M. and Yang, X.L. (2000) dFADD, a novel death domain-containing adapter protein for the *Drosophila* caspase DREDD. *J. Biol. Chem.*, **275**, 30761–30764.
 60. Kounatidis, I., Chtarbanova, S., Cao, Y., Hayne, M., Jayanth, D., Ganetzky, B. and Ligoxygakis, P. (2017) NF-kappa B immunity in the brain determines fly lifespan in healthy aging and age-related neurodegeneration. *Cell Rep.*, **19**, 836–848.
 61. Sears, C., Olesen, J., Rubin, D., Finley, D. and Maniatis, T. (1998) NF-kappa B p105 processing via the ubiquitin-proteasome pathway. *J. Biol. Chem.*, **273**, 1409–1419.
 62. Lemaitre, B. and Hoffmann, J. (2007) The host defense of *Drosophila melanogaster*. *Annu. Rev. Immunol.*, **25**, 697–743.
 63. Ligoxygakis, P. (2013) Genetics of immune recognition and response in *Drosophila* host defense. *Adv. Genet.*, **83**, 71–97.

64. Myllymaki, H., Valanne, S. and Ramet, M. (2014) The *Drosophila* IMD signaling pathway. *J. Immunol.*, **192**, 3455–3462.
65. Zhai, Z.Z., Huang, X.S. and Yin, Y.L. (2018) Beyond immunity: the IMD pathway as a coordinator of host defense, organismal physiology and behavior. *Dev. Comp. Immunol.*, **83**, 51–59.
66. Kaltschmidt, B. and Kaltschmidt, C. (2009) NF-kappa B in the nervous system. *Cold Spring Harb. Perspect. Biol.*, **1**, a001271.
67. Boersma, M.C. and Meffert, M.K. (2008) Novel roles for the NF-kappa B signaling pathway in regulating neuronal function. *Sci. Signal.*, **1**, pe7.
68. Meffert, M.K. and Baltimore, D. (2005) Physiological functions for brain NF-kappa B. *Trends Neurosci.*, **28**, 37–43.
69. Nguyen, M.D. (2002) Innate immunity: the missing link in neuroprotection and neurodegeneration? *Nat. Rev. Neurosci.*, **3**, 216–227.
70. Sochocka, M., Diniz, B.S. and Leszek, J. (2017) Inflammatory response in the CNS: friend or foe? *Mol. Neurobiol.*, **54**, 8071–8089.
71. Lubin, F.D. and Sweatt, J.D. (2007) The I kappa B kinase regulates chromatin structure during reconsolidation of conditioned fear memories. *Neuron*, **55**, 942–957.
72. Albensi, B.C. and Mattson, M.P. (2000) Evidence for the involvement of TNF and NF-kappa B in hippocampal synaptic plasticity. *Synapse*, **35**, 151–159.
73. Beattie, E.C., Stellwagen, D., Morishita, W., Bresnahan, J.C., Ha, B.K., Von Zastrow, M., Beattie, M.S. and Malenka, R.C. (2002) Control of synaptic strength by glial TNF alpha. *Science*, **295**, 2282–2285.
74. Nickols, J.C., Valentine, W., Kanwal, S. and Carter, B.D. (2003) Activation of the transcription factor NF-kappa B in Schwann cells is required for peripheral myelin formation. *Nat. Neurosci.*, **6**, 161–167.
75. Rolls, A., Shechter, R., London, A., Ziv, Y., Ronen, A., Levy, R. and Schwartz, M. (2007) Toll-like receptors modulate adult hippocampal neurogenesis. *Nat. Cell Biol.*, **9**, 1081–1088.
76. Chinchore, Y., Gerber, G.F. and Dolph, P.J. (2012) Alternative pathway of cell death in *Drosophila* mediated by NF-kappa B transcription factor relish. *Proc. Natl. Acad. Sci. U.S.A.*, **109**, E605–E612.
77. Heckscher, E.S., Fetter, R.D., Marek, K.W., Albin, S.D. and Davis, G.W. (2007) NF-kappa B, I kappa B, and IRAK control glutamate receptor density at the *Drosophila* NMJ. *Neuron*, **55**, 859–873.
78. Cao, Y., Chtarbanova, S., Petersen, A.J. and Ganetzky, B. (2013) Dnr1 mutations cause neurodegeneration in *Drosophila* by activating the innate immune response in the brain. *Proc. Natl. Acad. Sci. U.S.A.*, **110**, E1752–E1760.
79. Petersen, A.J., Katzenberger, R.J. and Wassarman, D.A. (2013) The innate immune response transcription factor relish is necessary for neurodegeneration in a *Drosophila* model of ataxia-telangiectasia. *Genetics*, **194**, 133.
80. Li, Y.X., Sibon, O.C.M. and Dijkers, P.F. (2018) Inhibition of NF-kappa B in astrocytes is sufficient to delay neurodegeneration induced by proteotoxicity in neurons. *J. Neuroinflammation*, **15**, 261.
81. Frakes, A.E., Ferraiuolo, L., Haidet-Phillips, A.M., Schmelzer, L., Braun, L., Miranda, C.J., Ladner, K.J., Bevan, A.K., Foust, K.D., Godbout, J.P. et al. (2014) Microglia induce motor neuron death via the classical NF-kappa B pathway in amyotrophic lateral sclerosis. *Neuron*, **81**, 1009–1023.
82. Bazan, N.G. (2009) Is NF-kappa B from astrocytes a decision maker of neuronal life or death? (commentary on Dvorianchikova et al.). *Eur. J. Neurosci.*, **30**, 173–174.
83. Kounatidis, I. and Chtarbanova, S. (2018) Role of glial immunity in lifespan determination: a *Drosophila* perspective. *Front. Immunol.*, **9**, 1362.
84. O'Rourke, J.G., Bogdanik, L., Yanez, A., Lall, D., Wolf, A.J., Muhammad, A.K., Ho, R., Carmona, S., Vit, J.P., Zarrow, J. et al. (2016) C9orf72 is required for proper macrophage and microglial function in mice. *Science*, **351**, 1324–1329.
85. Swarup, V., Phaneuf, D., Bareil, C., Robertson, J., Rouleau, G.A., Kriz, J. and Julien, J.P. (2011) Pathological hallmarks of amyotrophic lateral sclerosis/frontotemporal lobar degeneration in transgenic mice produced with TDP-43 genomic fragments. *Brain*, **134**, 2610–2626.
86. O'Neill, L.A.J. and Kaltschmidt, C. (1997) NF-kappa B: a crucial transcription factor for glial and neuronal cell function. *Trends Neurosci.*, **20**, 252–258.
87. Paquette, N., Broemer, M., Aggarwal, K., Chen, L., Husson, M., Erturk-Hasdemir, D., Reichhart, J.M., Meier, P. and Silverman, N. (2010) Caspase-mediated cleavage, IAP binding, and ubiquitination: linking three mechanisms crucial for *Drosophila* NF-kappa B signaling. *Mol. Cell*, **37**, 172–182.
88. Meinander, A., Runchel, C., Tenev, T., Chen, L., Kim, C.H., Ribeiro, P.S., Broemer, M., Leulier, F., Zvelebil, M., Silverman, N. et al. (2012) Ubiquitylation of the initiator caspase DREDD is required for innate immune signalling. *EMBO J.*, **31**, 2770–2783.
89. Kanekura, K., Suzuki, H., Aiso, S. and Matsuoka, M. (2009) ER stress and unfolded protein response in amyotrophic lateral sclerosis. *Mol. Neurobiol.*, **39**, 81–89.
90. Mori, A., Yamashita, S., Uchino, K., Suga, T., Ikeda, T., Takamatsu, K., Ishizaki, M., Koide, T., Kimura, E., Mita, S. et al. (2011) Derlin-1 overexpression ameliorates mutant SOD1-induced endoplasmic reticulum stress by reducing mutant SOD1 accumulation. *Neurochem. Int.*, **58**, 344–353.
91. Kuijpers, M., Yu, K.L., Teuling, E., Akhmanova, A., Jaarsma, D. and Hoogenraad, C.C. (2013) The ALS8 protein VAPB interacts with the ER-Golgi recycling protein YIF1A and regulates membrane delivery into dendrites. *EMBO J.*, **32**, 2056–2072.
92. Fasana, E., Fossati, M., Ruggiano, A., Brambillasca, S., Hoogenraad, C.C., Navone, F., Francolini, M. and Borgese, N. (2010) A VAPB mutant linked to amyotrophic lateral sclerosis generates a novel form of organized smooth endoplasmic reticulum. *FASEB J.*, **24**, 1419–1430.
93. Vembar, S.S. and Brodsky, J.L. (2008) One step at a time: endoplasmic reticulum-associated degradation. *Nat. Rev. Mol. Cell Biol.*, **9**, 944–957.
94. Moumen, A., Virard, I. and Raoul, C. (2011) Accumulation of wildtype and ALS-linked mutated VAPB impairs activity of the proteasome. *PLoS One*, **6**, e26066. doi: [10.1371/journal.pone.0026066](https://doi.org/10.1371/journal.pone.0026066).
95. Diaper, D.C., Adachi, Y., Lazarou, L., Greenstein, M., Simoes, F.A., Di Domenico, A., Solomon, D.A., Lowe, S., Alsubaie, R., Cheng, D. et al. (2013) *Drosophila* TDP-43 dysfunction in glia and muscle cells cause cytological and behavioural phenotypes that characterize ALS and FTL. *Hum. Mol. Genet.*, **22**, 3883–3893.
96. Lee, B.P. and Jones, B.W. (2005) Transcriptional regulation of the *Drosophila* glial gene repo. *Mech. Dev.*, **122**, 849–862.
97. Handu, M., Kaduskar, B., Ravindranathan, R., Soory, A., Giri, R., Elango, V.B., Gowda, H. and Ratnaparkhi, G.S. (2015) SUMO-enriched proteome for *Drosophila* innate immune response. *G3-Genes Genom. Genet.*, **5**, 2137–2154.
98. Shevchenko, A., Tomas, H., Havlis, J., Olsen, J.V. and Mann, M. (2006) In-gel digestion for mass spectrometric characterization of proteins and proteomes. *Nat. Protoc.*, **1**, 2856–2860.
99. Rappsilber, J., Mann, M. and Ishihama, Y. (2007) Protocol for micro-purification, enrichment, pre-fractionation and storage

- of peptides for proteomics using stage tips. *Nat. Protoc.*, **2**, 1896–1906.
100. Madabattula, S.T., Strautman, J.C., Bysice, A.M., O'Sullivan, J.A., Androschuk, A., Rosenfelt, C., Doucet, K., Rouleau, G. and Bolduc, F. (2015) Quantitative analysis of climbing defects in a *Drosophila* model of neurodegenerative disorders. *J. Vis. Exp.*, **13**, e52741.
101. Branco, J., Al-Ramahi, I., Ukani, L., Perez, A.M., Fernandez-Funez, P., Rincon-Limas, D. and Botas, J. (2008) Comparative analysis of genetic modifiers in *Drosophila* points to common and distinct mechanisms of pathogenesis among polyglutamine diseases. *Hum. Mol. Genet.*, **17**, 376–390.
102. Azuma, Y., Tokuda, T., Shimamura, M., Kyotani, A., Sasayama, H., Yoshida, T., Mizuta, I., Mizuno, T., Nakagawa, M., Fujikake, N. et al. (2014) Identification of *ter94*, *Drosophila* VCP, as a strong modulator of motor neuron degeneration induced by knockdown of *Caz*, *Drosophila* FUS. *Hum. Mol. Genet.*, **23**, 3467–3480.